OXFORD

Human Molecular Genetics, 2024, 1–19
https://doi.org/10.1093/hmg/ddae094
Original Article

Ablation of the dystrophin Dp71f alternative C-terminal variant increases sarcoma tumour cell aggressiveness

Nancy Alnassar[1], Jacek Hajto[2], Robin M.H. Rumney[1], Suraj Verma[3], Malgorzata Borczyk[2], Chandrika Saha[1], Janos Kanczler[4], Arthur M. Butt[1], Annalisa Occhipinti[3], Joanna Pomeroy[1], Claudio Angione[3], Michal Korostynski[2], Dariusz C. Górecki[1,*]

[1]School of Pharmacy and Biomedical Sciences, University of Portsmouth, White Swan Road, Portsmouth PO1 2DT, United Kingdom
[2]Laboratory of Pharmacogenomics, Maj Institute of Pharmacology PAS, Smetna 12, Krakow 31155, Poland
[3]School of Computing, Engineering and Digital Technologies, Teesside University, Middlesbrough, Tees Valley TS1 3BX, United Kingdom
[4]Bone & Joint Research Group, Department of Human Development and Health, University of Southampton, Tremona Road, Southampton SO16 6YD, United Kingdom

*Corresponding author. School of Pharmacy and Biomedical Sciences, University of Portsmouth, White Swan Road, Portsmouth PO1 2DT, United Kingdom. E-mail: darek.gorecki@port.ac.uk

Abstract

Alterations in Dp71 expression, the most ubiquitous dystrophin isoform, have been associated with patient survival across tumours. Intriguingly, in certain malignancies, Dp71 acts as a tumour suppressor, while manifesting oncogenic properties in others. This diversity could be explained by the expression of two Dp71 splice variants encoding proteins with distinct C-termini, each with specific properties. Expression of these variants has impeded the exploration of their unique roles. Using CRISPR/Cas9, we ablated the Dp71f variant with the alternative C-terminus in a sarcoma cell line not expressing the canonical C-terminal variant, and conducted molecular (RNAseq) and functional characterisation of the knockout cells. Dp71f ablation induced major transcriptomic alterations, particularly affecting the expression of genes involved in calcium signalling and ECM-receptor interaction pathways. The genome-scale metabolic analysis identified significant downregulation of glucose transport via membrane vesicle reaction (GLCter) and downregulated glycolysis/gluconeogenesis pathway. Functionally, these molecular changes corresponded with, increased calcium responses, cell adhesion, proliferation, survival under serum starvation and chemotherapeutic resistance. Knockout cells showed reduced GLUT1 protein expression, survival without attachment and their migration and invasion *in vitro* and *in vivo* were unaltered, despite increased matrix metalloproteinases release. Our findings emphasise the importance of alternative splicing of dystrophin transcripts and underscore the role of the Dp71f variant, which appears to govern distinct cellular processes frequently dysregulated in tumour cells. The loss of this regulatory mechanism promotes sarcoma cell survival and treatment resistance. Thus, Dp71f is a target for future investigations exploring the intricate functions of specific *DMD* transcripts in physiology and across malignancies.

Keywords: Dp71f; tumour; Duchenne muscular dystrophy; alternative C-terminus; Ewing sarcoma

Introduction

The *DMD* gene is the second largest human gene known, with 79 exons spanning ∼2.3 Mb, eight independent tissue-specific promoters, and extensive alternative splicing adding further complexity [1, 2]. Its name reflects its causative role in Duchenne muscular dystrophy, and it has been investigated primarily in the context of this neuromuscular disease. However, the *DMD* gene function is already evident in the developing mesoderm [3] and we have recently demonstrated that the dystrophin protein has housekeeping characteristics [4]. Importantly, alterations in the expression of *DMD* transcript variants distinguished malignant from control samples across 25 different types of primary tumours [4], and expression levels of specific *DMD* transcripts can serve as a biomarker for predicting patient survival across different tumour types [4, 5]. Our findings consolidate the emerging view on the role of this gene in malignancy [6]. Although instances of tumours in DMD patients are rarely reported, this may be attributed to their significantly reduced lifespan [7]. Notably, the typical dystrophic abnormalities include altered cell proliferation [8–10], migration [9, 11], and calcium signalling [12–14].

Moreover, pathological similarities notwithstanding, specific *DMD* transcripts may have distinct roles in various tumours [6]. This reflects the expression complexity of the *DMD* gene, with tissue-specific promoters driving distinct transcripts encoding specific dystrophin isoforms [15]. Three promoters control the expression of 14-kb full-length transcripts encoding 427 kDa dystrophins (Dp427). Further intragenic promoters give rise to transcripts encoding truncated isoforms, of which Dp71 is driven by a housekeeping-type promoter [16] and is the most ubiquitous in terms of its tissue distribution [1].

Loss of Dp427 was found to enhance the metastatic potential of myogenic tumours [17]. Moreover, expression of this transcript was found downregulated in 68% of tumours compared to control tissues [4].

On the other hand, the impact of Dp71 in tumours is equivocal. It acts as a positive regulator of cell viability in various sarcomas and lung adenocarcinoma [17–19]. Conversely, reduced Dp71

Received: December 29, 2023. **Revised:** May 8, 2024. **Accepted:** May 30, 2024

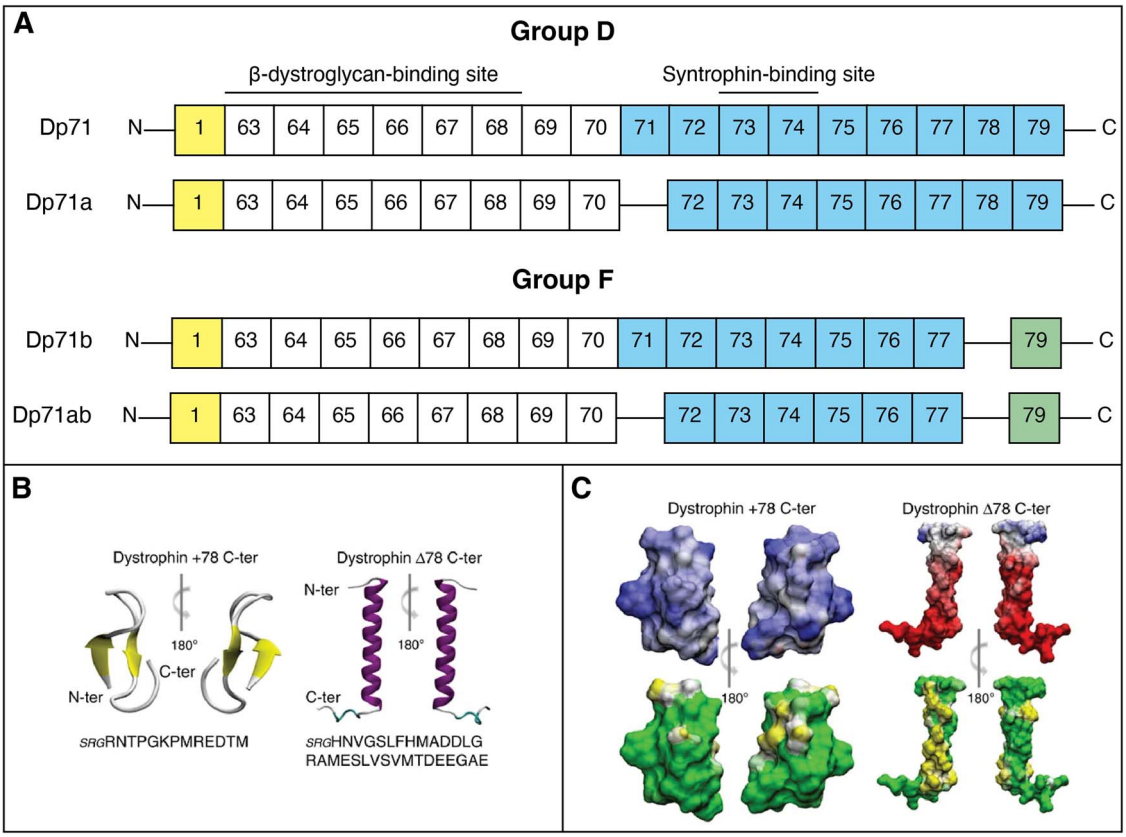

Figure 1. (A) Schematic representation of Dp71 splice variants grouped according to their C-terminal domain (blue). Group D (Dp71d) contains exons 78 and 79, while group F (Dp71f) is characterised by the absence of exon 78 and the presence of an alternative exon 79 (green). The binding sites for DAPC proteins β-dystroglycan and syntrophin are illustrated. (B) The peptide structure predicted from the amino acid sequence for +78 and −78 exon-encoded C-terminal domains. Panels B and C were obtained from [25], creative commons attribution 4.0 international license. (C) Upper panel: The electrostatic surface potentials (blue for positive and red for negative) of the +78 and −78 C-terminal domains. Lower panel: The hydrophobic (yellow) and hydrophilic (green) surface potentials [25].

expression is associated with increased proliferation of glioblastoma [20], and forced overexpression of Dp71 resulted in reduced gastric adenocarcinoma cell proliferation [21]. This divergence is also seen in the survival data. In gastric adenocarcinoma [21], haematological malignancies [4] and leiomyosarcomas (Alnassar *et al*, unpublished data), high expression of Dp71 is associated with longer survival, but in low-grade gliomas [22], mesotheliomas [5] and non-myogenic sarcomas (Alnassar *et al*, unpublished data), it is linked to poor survival.

The diverse roles of Dp71, acting as a putative oncogenic factor in some tumours and a tumour suppressor in others, might be attributed to the distinct expression patterns of various Dp71 splice variants within different tumours. Dp71 mRNA is characterised by multiple alternative splicing events [23]. The main types result from alternative splicing of exons 71 and 78 (Fig. 1A). Dp71a lacks exon 71, Dp71b lacks exon 78, and Dp71ab lacks both exons. The absence of exon 71, results in the removal of 13 amino acids that does not alter the reading frame [24]. However, the loss of exon 78 leads to a complete reorganisation of the molecular structure of the C-terminus through the replacement of the 17-aa β-sheet hydrophilic C-terminus that has a global positive charge with an alternative 31-aa amphipathic α-helix hydrophobic one with a global negative charge (Fig. 1B and C) [24, 25]. Notably, the 31-aa-sequence encoding the hydrophobic C-terminus is highly conserved from nematode to human, suggesting a critical function for this domain [26]. This C-terminal structure is often used to classify Dp71 variants into the Dp71d and Dp71f groups with the canonical and alternative C-terminal domains, respectively [27].

Variants containing or lacking exon 78 have different subcellular distributions and can have distinct functions [8, 28–32]. Dp71, through its C-terminus and cysteine-rich domain, interacts with β-dystroglycan and syntrophin to form the dystrophin-associated protein complex (DAPC) in the plasma membrane and/or cell nucleus [23, 28, 33–35]. These complexes are involved in cell adhesion [34, 36–38], and through Lamin B1 and β-dystroglycan, play a role in cell division [19–21, 35].

Splicing may also alter important phosphorylation events. The cyclin-dependent kinase 1 (CDK1) phosphorylates Dp71 at a site encoded by exon 78 [24]. The Ca^{2+}/calmodulin-dependent protein kinase II (CaMKII)-mediated phosphorylation at a site encoded by exon 79 was proposed to modulate the nuclear localisation of Dp71 [39]. Both these sites are not present in the unique C-terminus translated from the Dp71f variants. Differential expression of these distinct splice variants, with different localisation and interactions with actin and DAPC components could explain the diverse, often opposing effects evoked by Dp71 in various malignancies. However, the functional investigation of Dp71 splice variants in tumours has been hindered by their co-expression [27, 31, 40].

Therefore, we identified a tumour cell line expressing the Dp71f splice variant group only, ablated its expression using CRISPR/-Cas9 and performed molecular and functional characterisation of the resulting knockout cells.

Table 1. KEGG pathways enriched in the DEGs between Dp71f knockout cells and non-targeting controls.

Pathway	Adjusted P-value	Genes
Calcium signalling pathway	0.019	RET, PDE1B, PDE1A, ADCY4, ITPR1, CXCR4, ADCY2, CACNA1C, GRPR, ADCY7, ADRA1A, GRIN2A, CYSLTR1, HRH1, CCKAR, PPP3CC, KDR, PLCG2, DRD1, NOS1, FGF22, PDGFRA, NOS2, NOS3, MST1, AVPR1A, GRIN2C, GRIN2D, TRDN, ADORA2A, P2RX2, P2RX1, ORAI3, FGF18, HRC, CASQ2, FGFR2
ECM-receptor interaction	0.046	LAMA5, ITGA4, SDC4, ITGB4, ITGA1, LAMA3, NPNT, THBS2, THBS1, COL1A1, SV2C, ITGA11, SPP1, ITGA6, FREM1, FREM2, ITGA9
Dilated cardiomyopathy	0.046	TGFB1, ITGA4, ITGB4, TPM2, ITGA1, ADCY4, ADCY2, CACNA2D4, CACNA1C, ADCY7, ADCY6, MYL3, ITGA11, ITGA6, TNNI3, CACNG4, ITGA9, CACNG5

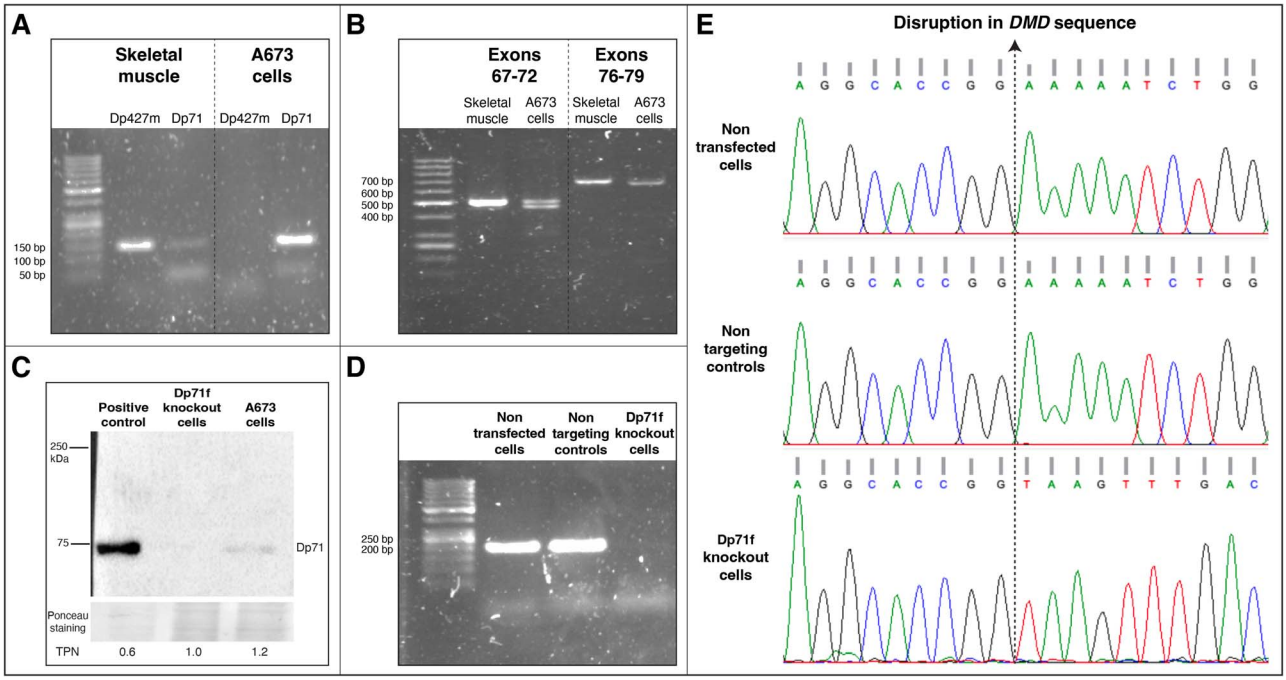

Figure 2. Generation of Dp71f knockout cells. (A) Expression of Dp427m and Dp71 transcripts in A673 cells and skeletal muscle (positive control) using primer pairs 2 and 3, respectively. (B) Expression of Dp71 splice variants in A673 cells and skeletal muscle (positive control) using primer pairs 4 and 5 for exon 71 and 78 splicing, respectively. (C) Western blot showing Dp71 protein expression in mouse cerebellum (positive control), A673 but not Dp71f knockout cells. Confirmation of successful knockout by PCR using primer pair 1 (D) showing the loss of *DMD* expression in knockout cells compared to non-transfected and non-targeting controls and (E) by sanger sequencing showing a disruption in the *DMD* gene sequence in the knockout cells.

Results

Generation of Dp71f knockout Ewing sarcoma cells

According to RNAseq data at the DepMap portal, among the various *DMD* gene transcripts, Dp71b, encoding the alternative C-terminus, exhibits the highest expression in the A673 cell line, which lacks the expression of Dp427m. Moreover, the mass-spectrometry-based protein expression data indicated the presence of dystrophin protein in A673 cells. We verified the expression of *DMD* transcripts in the A673 cell line in a PCR assay using transcript-specific primer pairs (Table 1), which confirmed that A673 cells express Dp71 but not Dp427m (Fig. 2A). Next, we characterised the Dp71 splice variants expressed in A673 cells using primers that amplify sequences spanning exons 71 and 78 (Table 1; primer pairs 4 and 5), which confirmed that these cells only express variants lacking exon 78, thus encoding an alternative C-terminus. We also found exon 71 splicing in a proportion of the transcripts. This was corroborated further by RNAseq analysis (see below). Therefore, we established that A673 cells only express Dp71f (Fig. 2B) but not variants encoding the canonical C-terminus. The Dp71 protein in A673 cells was detectable using Western blotting, albeit at a very low level (Fig. 2C).

We knocked out the Dp71f transcripts using a sgRNA targeting exon 69. Single cell clones were collected, and the successful knockout was confirmed using PCR (Fig. 2D), Sanger sequencing (Fig. 2E), and at the protein level (Fig. 2C).

Ablation of Dp71f expression causes specific transcriptomic alterations

RNA extracted from knockout, non-targeting control and non-transfected cells was analysed by RNA sequencing. Mapping the RNAseq reads to identify splicing events of exons 71, 72, 77 and 78 in non-transfected A673 cells confirmed that exon 78 retention was a very rare event or not found at all, while exon 71 was often spliced out. Exons 72 and 77 were always present. (Supplementary Fig. 4).

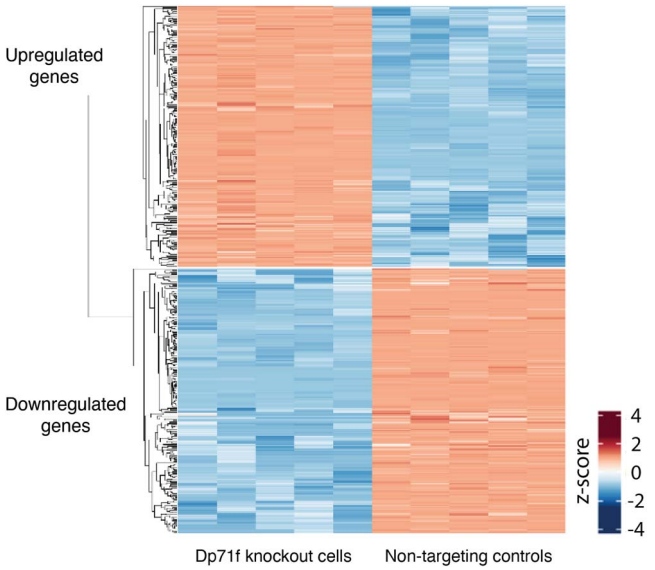

Figure 3. Heatmap of the DEGs between Dp71f knockout cells and non-targeting controls. Clustering revealed two groups of genes: Up- and downregulated. The FDR for group comparison was < 0.001 and absolute $Log_2FC \geq 2$. Gene abundance is represented as z-scores for log_2-transformed gene count values. Red colours indicate expression above the mean for each gene and blue colours indicate decreased abundance.

Furthermore, we identified 1579 DEGs between the Dp71f knockout cells and non-targeting controls (Fig. 3, full results available in Supplementary Tables File 1).

Three pathways were enriched in these DEGs (Table 1): calcium signalling ($P = 0.019$), ECM-receptor interaction ($P = 0.046$), and dilated cardiomyopathy ($P = 0.046$). The DEGs between non-targeting controls and non-transfected cells did not exhibit enrichment in any of the three pathways, confirming that these alterations are specifically induced by the loss of Dp71f expression and not by the cell transfection or selection procedures.

The dilated cardiomyopathy is a key life-limiting condition in DMD [41] and the DEGs in this pathway overlap heavily with the ECM-interaction and also, to a lesser extent, with the calcium signalling pathway (Table 1). Alterations of calcium homeostasis and extracellular matrix interactions are well-known abnormalities resulting from *DMD* mutations [14, 42, 43], but are also major abnormalities in tumours [44–46]. Therefore, we performed in-depth functional analyses to verify the impact of these alterations.

Metabolic pathway alteration in Dp71f knockout cells

Given the metabolic alterations identified in dystrophic myoblasts and brains [9, 47], we created a genome-wide metabolic model (GSMM) comparing the Dp71f knockout and non-targeting control cells. Figure 4 and Supplementary Tables File 2 illustrate the metabolic activity FC (expressed in log_2FC) across reactions in the constrained metabolic model. We found a significant downregulation of the glycolysis/gluconeogenesis pathway ($log_2FC = -0.6585$) and hexokinase 1 (HEX1) reaction ($log_2FC = -0.053$) in this pathway in knockout cells compared to non-targeting controls. The glucose transport *via* membrane vesicle reaction (GLCter) linked with the SLC2A1 gene encoding the GLUT1 protein was found to be downregulated ($log_2FC = -1.14$). Moreover, downregulated glutamate 5-kinase (GLU5Km; $log_2FC = -5.6269$) and glutamate-5-semialdehyde dehydrogenase (G5SDym; $log_2FC = -5.6269$) reactions in the arginine and proline metabolism pathway were evident in knockout cells. On the other hand, there was upregulation of phosphatidylserine decarboxylase (PSDm_hs; $log_2FC = 5.28$) in the mitochondrial glycerophospholipid metabolism pathway.

Given that GLUT1 is the key protein involved in glucose transport in the GLCter reaction, we evaluated its expression using Western blotting. GLUT1 levels were significantly decreased ($P = 0.046$) in Dp71f knockouts compared to non-targeting control cells (Fig. 5).

Ablation of Dp71f expression alters calcium signalling

As we identified alterations in P2X receptors expression in dystrophin-null cells (Table 1), and purinergic abnormalities are a well-known effect of *DMD* mutations (reviewed in [48]), we employed ATP as a P2X agonist to evoke calcium signals. The calcium response after the addition of ATP was significantly higher in in Fluo-4 loaded knockout cells than in non-targeting controls ($P = 0.0032$), thus confirming the role of Dp71f in calcium signalling (Fig. 6, Supplementary Movies).

Ablation of Dp71f expression increases cell proliferation

Since calcium signalling plays a key role in controlling cell division [49], we compared cell proliferation between knockout and control cells using two approaches. Under the normal (10% FBS) serum condition, loss of Dp71f expression increased cell proliferation. The PrestoBlue™ assay (Fig. 7A) showed significantly higher values for knockout cells than controls ($P = 0.0004$). Furthermore, the crystal violet staining for assessing cell numbers as stained areas (Fig. 7B) and OD_{570} values of the solubilised crystal violet dye (Fig. 7C) showed significantly higher values for knockout than non-transfected cells ($P = 0.0014$ and $P = 0.0003$, respectively) and non-targeting controls ($P = 0.0001$ and $P = 0.0007$, respectively. Under low (2% FBS) serum condition, Dp71f-null cells also showed increased cell proliferation compared to non-transfected cells and non-targeting controls (Supplementary Fig. 1).

Ablation of Dp71f expression decreases apoptosis in response to serum deprivation

As Dp71f knockout cells proliferated in low serum conditions, we assessed their survival in response to serum deprivation. Serum deprivation for 48 h led to increased apoptosis (Fig. 8; Supplementary Fig. 2) in both knockout cells ($P < 0.0001$) and non-targeting controls ($P < 0.0001$). However, the percentage of apoptotic cells was significantly lower for Dp71f knockout cells compared to non-targeting controls ($P < 0.0001$).

Loss of Dp71f expression enhances the colony-forming ability

Given that the capacity of single cells to survive and form colonies is another tumour hallmark, we compared the knockout and control cells in the clonogenic assay. When seeded at a density of 1000 cells per 9.6 cm^2 (6-well plate), both non-transfected and non-targeting control cells formed only a few colonies over the two-week period. In contrast, individual knockout cells survived, proliferated, and expanded into numerous clonal populations (Fig. 9A). The number of colonies formed by knockout cells (Fig. 9B) was significantly higher than non-transfected ($P = 0.0006$) and non-targeting control cells ($P = 0.0059$).

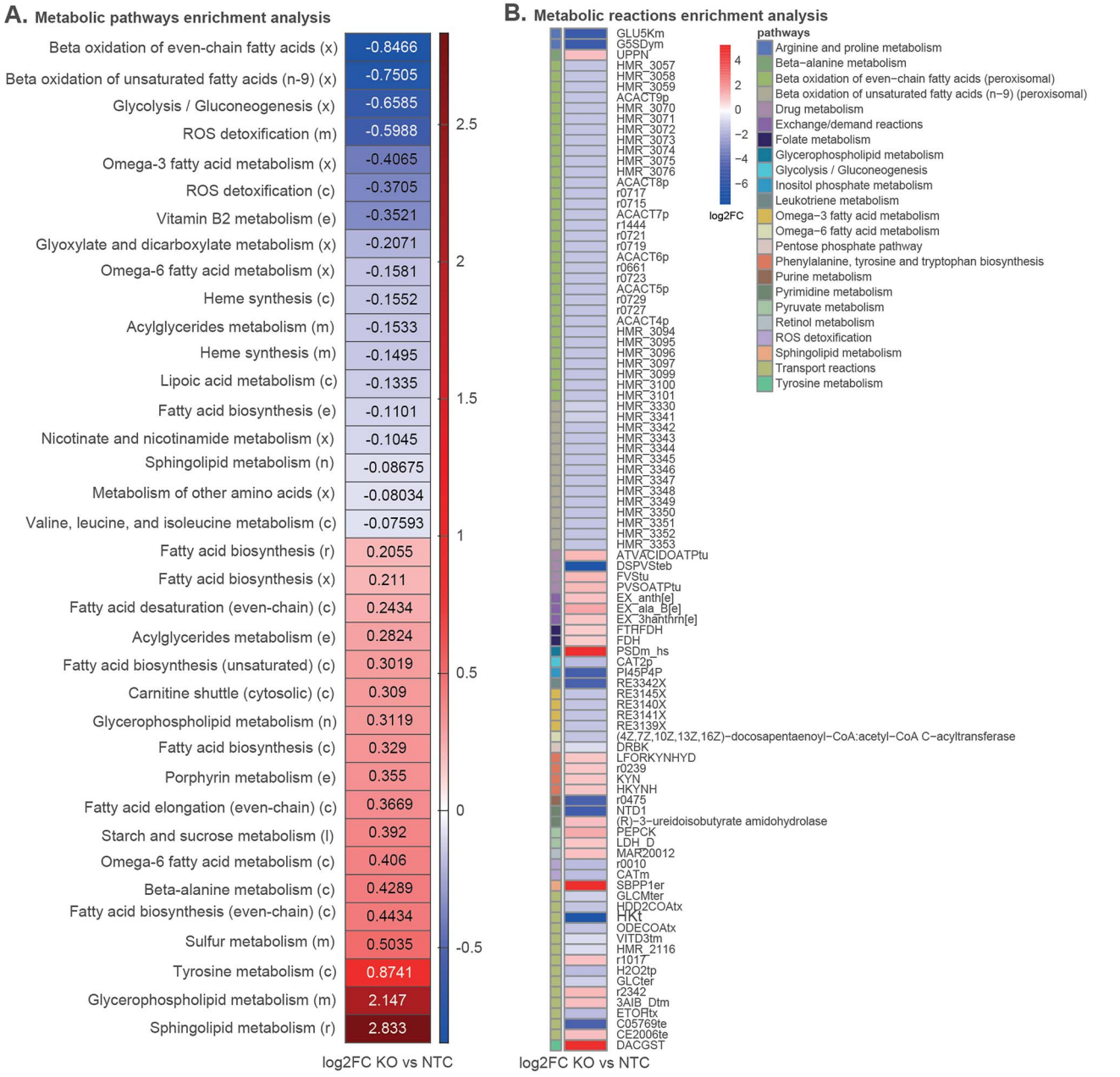

Figure 4. Metabolic alterations between Dp71f knockout (KO) cells and non-targeting controls (NTC) (A). Enriched metabolic pathways and (B). Enriched metabolic reactions. The reactions are grouped by their respective pathways. The upregulated pathways/reactions highlighted in red and downregulated shown in blue.

Knockout of Dp71f expression increases cell adhesion and *anoikis*

The DEGs between knockout cells and non-targeting controls indicated an alteration in the ECM-receptor interaction pathway. Since cell adhesion plays a significant role in determining the tumour metastatic potential, we evaluated the effect of Dp71f knockout on adhesion to non-coated and ECM-coated cell culture plates over 2 h. The phase contrast microscopy images showed that knockout cells displayed more robust adhesion and spreading compared with non-transfected and non-targeting controls on both non-coated (Fig. 10A) and ECM-coated (Fig. 10B) surfaces.

In the non-coated plates, Dp71f knockout cells adhered significantly stronger than both non-transfected cells and non-targeting controls ($P < 0.0001$; Fig. 10C) as measured by the crystal violet-stained cell areas and the colorimetric assay. Similarly, when cells were seeded on Geltrex™, the area of stained cells as well as the OD_{570} values of the solubilised crystal violet were significantly higher for knockout cells compared to both controls ($P < 0.0001$; Fig. 10D). Therefore, Dp71f knockout cells adhere more strongly.

Given that the loss of Dp71f expression increases cell adhesion, we assessed whether knockout cells cope differently when unable to adhere. To do this, we compared *anoikis*, a form of programmed cell death in response to the loss of cell-matrix interactions [50]. While the loss of attachment increased *anoikis* (Fig. 10E; Supplementary Fig. 2) in both knockout ($P < 0.0001$) and non-targeting control cells ($P < 0.0001$), *anoikis* was significantly higher in Dp71f knockouts ($P < 0.0001$). This shows that the stronger adhesion of Dp71f knockout cells helps their survival.

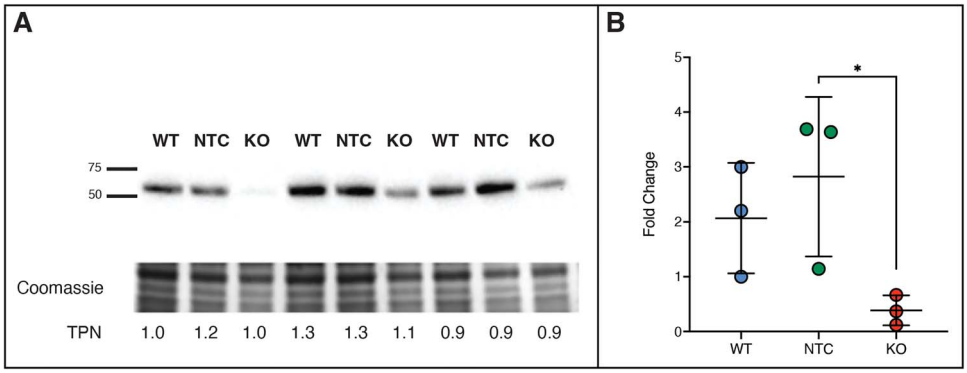

Figure 5. GLUT1 protein expression in Dp71f knockout cells and controls. (A) An example western blot of GLUT1 protein expression in non-transfected (WT), non-targeting controls (NTC) and Dp71f knockout A673 cells (KO). Bottom panel—Corresponding Coomassie-stained protein bands. The total protein normalisation (TPN) values represent optical density of each band normalized to the total protein in the corresponding CBB-stained lane. B. Fold change data presented as mean ± SD (n = 3 per group).

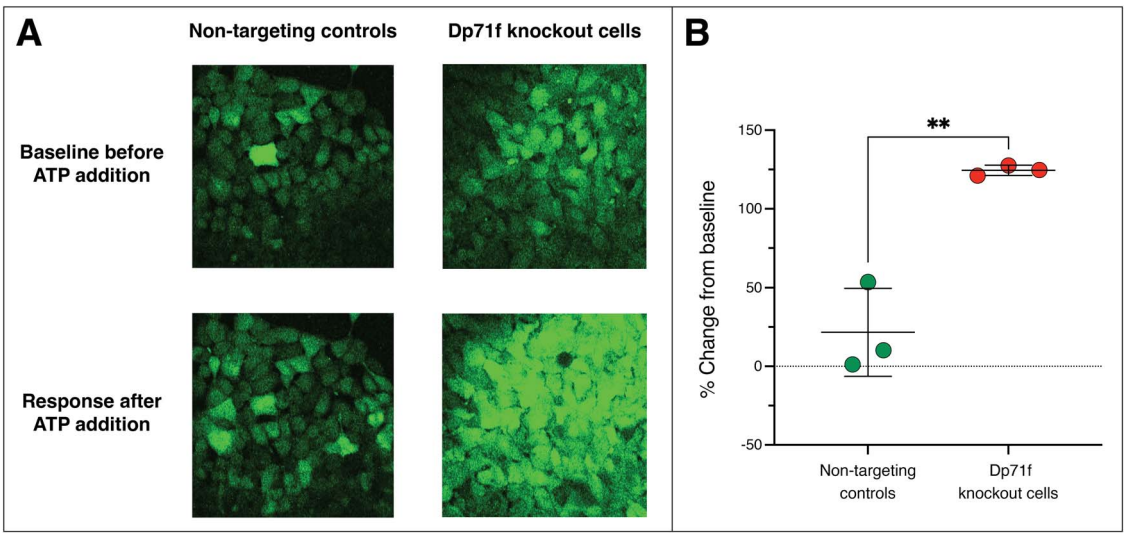

Figure 6. Calcium signalling is increased in Dp71f knockout cells. (A) Confocal images of the fluorescence intensity of the cytosolic calcium dye Fluo-4 before and after the addition of ATP. (B) Change in fluorescence intensity after the addition of ATP compared to baseline. Data is presented as mean ± SD (n = 3 per group).

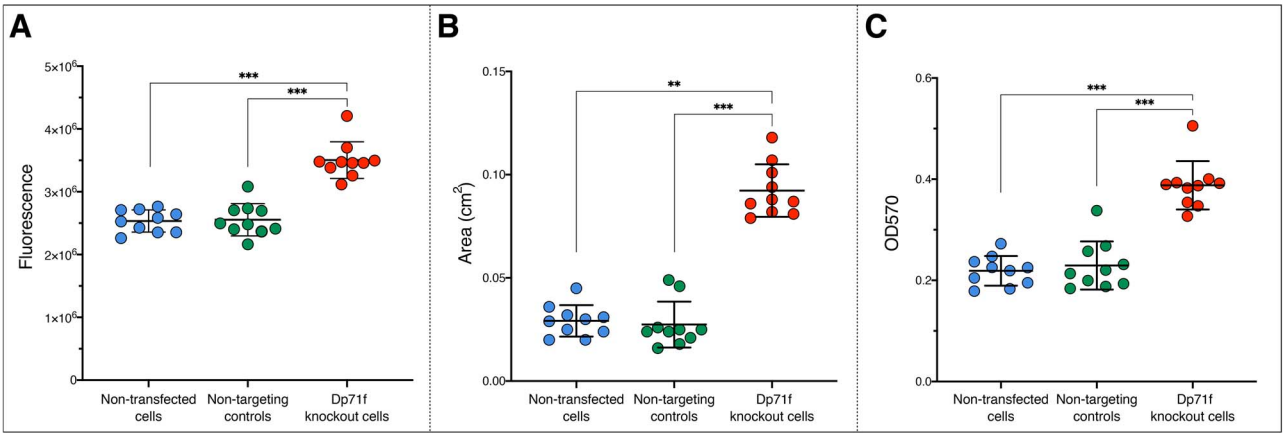

Figure 7. Proliferation is increased in Dp71f knockout cells. (A) Fluorescence measurements in the PrestoBlue™ cell viability assay. (B) Area of stained cells in cm^2. (C) OD_{570} measurements of the solubilised crystal violet dye. Data is presented as mean ± SD (n = 10 per group).

Ablation of Dp71f expression does not affect cell migration and invasion *in vitro*

Since both calcium signalling and ECM interactions play a role in regulating cell migration, the migratory ability of cells was investigated in the Boyden chamber assay (Fig. 11). No significant differences in cell migration were identified between knockout and control cells ($P = 0.434$ for area measurements and $P = 0.9281$ for absorbance measurements).

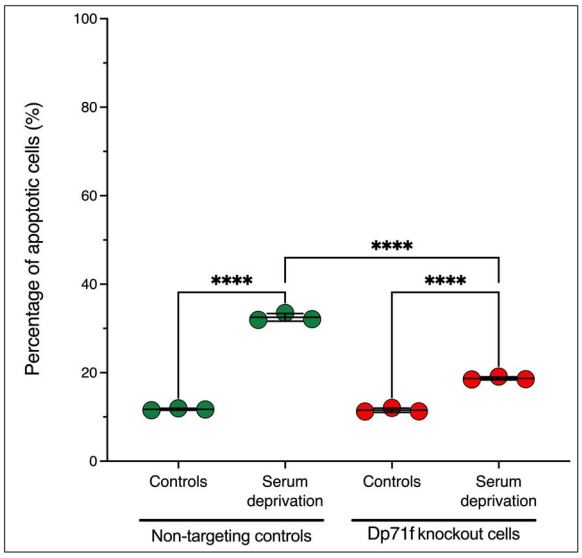

Figure 8. Apoptosis following serum deprivation is lower in Dp71f knockout. Data is presented as mean ± SD (n = 3 per group).

The wound healing assay attempts were thwarted by poor adhesion of control cells. While they formed a confluent monolayer, subsequent wound scratching led to the detachment of large areas in both non-transfected and non-targeting control cells (Supplementary Fig. 3), resulting in non-uniform wound formation and rendering comparisons impossible. However, this supported our findings of a significantly increased attachment of the Dp71f knockout compared to unmodified cells.

The transwell invasion assay (Fig. 12) showed no significant difference in the ability to invade a basement membrane matrix between knockout cells and controls ($P = 0.295$ for area measurements and $P = 0.9847$ for absorbance measurements).

Increased release of active MMP9 and MMP2 from Dp71f knockout cells

The lack of effect of Dp71f knockout on migration and invasion contrasts with findings in dystrophic myoblasts lacking either Dp427 or all dystrophins, which showed significantly altered chemotaxis [9] Given that increased matrix metalloproteinases MMP2 and MMP9 activity has been reported in dystrophic muscle and cells [51, 52], the zymography assay was performed. We found that Dp71f knockout cells released more active MMP9 and MMP2 into the media compared to non-transfected ($P < 0.0001$ and $P = 0.0127$, respectively) and non-targeting controls ($P < 0.0001$ and $P = 0.0086$, respectively; Fig. 13).

Dp71f knockout does not affect cell invasion or angiogenic capacity in the CAM assay

Given that no differences in cell invasion were found despite the presence of increased MMP9 and MMP2 activities in knockout cells, we used the CAM assay to assess the invasion, metastatic and angiogenic capabilities of knockout cells *in vivo*. Figure 14A shows images of fluorescently labelled cells that migrated from the seeding site across each CAM membrane. No statistically significant differences in area fraction measurements were identified ($P = 0.1747$; Fig. 14B) suggesting that Dp71f knockout does not affect invasion in this *in vivo* system. We also found no statistically significant differences in the Chalkley score values, and therefore, in the angiogenic capabilities of knockout compared to control cells ($P = 0.7498$; Fig. 14C).

Loss of Dp71f expression reduces sensitivity to etoposide

To determine whether Dp71f knockout alters the cell response to chemotherapeutic agents, we measured the effect of etoposide, a compound used in sarcoma treatment regimens [53]. Cells were exposed to increasing concentrations of etoposide and sigmoidal dose–response curves (Fig. 15A) were used to calculate the IC_{50} values (Fig. 15B). Dp71f knockout cells showed lower sensitivity to etoposide compared to non-transfected cells ($P < 0.0001$) and non-targeting controls ($P < 0.0001$).

Discussion

Recent studies have demonstrated the involvement of dystrophin Dp71 in tumours, and that its role varies depending on the tumour type [4, 6, 19–21, 23]. This variability could be explained by the involvement of two functionally different Dp71 isoforms resulting from the alternative splicing at the 3′-end. Dp71f mRNA encodes an alternative C terminus with different electrostatic and solubility properties and binding domains [24, 25]. The functional importance of this C-terminus is evident, as demonstrated by its forced inclusion, which impaired muscle structure and function in both zebrafish and mice. Additionally, the abnormal splicing of exon 78 observed in muscles of myotonic dystrophy patients correlated with identical ultrastructural abnormalities [25].

In this study, we specifically investigated the role of Dp71f by knocking it out in a sarcoma cell line in which only the transcripts with the alternative C-terminus were detected. Considering that this variant is produced through alternative splicing, a process known for its dynamic nature, the possibility of low-level expression of the canonical variant could not be ruled out entirely. However, mapping the RNAseq reads to identify splicing events of exons 71 to 78 in non-transfected A673 cells revealed that while exons 72 and 77 are always present in A673 cells, exon 78 is spliced out and exon 71 is often spliced out (Supplementary Fig. 4). Therefore, due to its rarity, any functional effect of the exon 78-containing transcript is expected to be minimal. This is confirmed by the absence of transcriptomic or functional differences between the individual A673 clones.

This study did not explore the potential impact of exon 71 presence or absence in Dp71 transcripts. Although it cannot be ruled out entirely, previous research has not associated the in-frame deletion of the 13 amino acids encoded by this exon with significant functional alterations [54].

The DEGs between Dp71f knockout cells and controls showed enrichment in calcium signalling and ECM-receptor interaction pathways, which are known to be altered in Duchenne patients [14, 42, 43] as well as in tumours [44–46]. Unexpectedly, the DEGs also showed enrichment in the dilated cardiomyopathy pathway, which is the leading cause of death in DMD [41, 55]. Thus, cardiomyopathy might potentially be exacerbated in rare dystrophin-null patients or in cases of aberrant exon 78 splicing, as shown by [25].

Dp71f knockout cells showed significantly elevated calcium responses when exposed to ATP, a purinergic receptor agonist [56] released in substantial amounts due to cell damage [57, 58]. This resembles the abnormal purinergic responses in Dp427-deficient muscle and lymphoblasts [12, 14, 59]. These parallel disruptions in calcium signalling may imply a commonality in molecular mechanisms evoked by Dp71 and Dp427 transcripts.

Notably, calcium signalling plays an essential role in regulating cell proliferation [49], adhesion [60, 61], migration and invasion

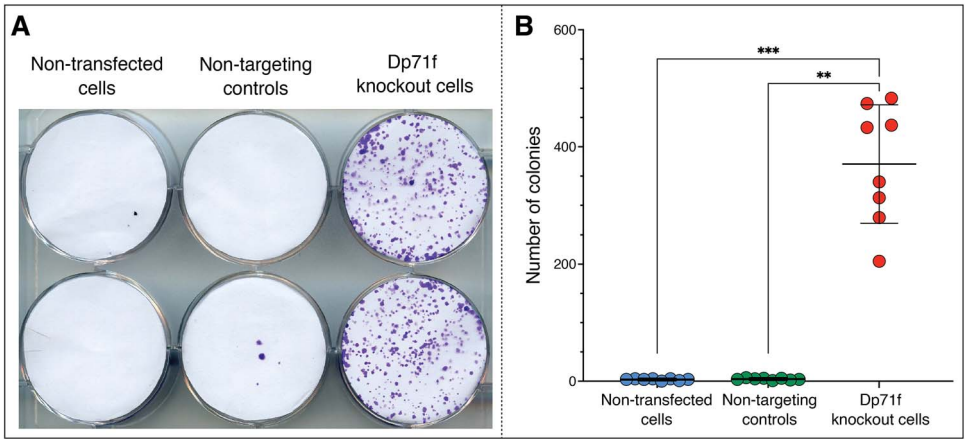

Figure 9. Colony formation is increased in Dp71f knockout cells. (A) Typical examples of colony formation in the clonogenic assay. Colonies were stained with crystal violet. (B) The number of colonies. Data is presented as mean ± SD (n = 8 per group from four independent replicate plates).

[62, 63], death [64], and resistance to treatment [63]—processes we found altered in Dp71f knockout cells.

The knockout of Dp71f leads to an increase in cell proliferation and their ability to grow as isolated colonies. This aligns with observations in glioblastoma, where reduced Dp71 expression inversely correlates with the Ki-67 proliferative index [20], while other studies reported reduced proliferation following Dp71 inhibition [17–19]. However, these studies did not discriminate between the Dp71 splice variants expressed in the analysed cells, whereas in glioblastoma cells, Dp71f was identified as the most abundant [40]. While strong exogenous overexpression of either Dp71d or Dp71f from a CMV promoter-driven plasmid reduced cancer cell proliferation [21], the effects observed in this study might result from the overexpression process itself. Cells finely regulate the expression of each protein, and the overexpression of wild-type genes can sometimes cause the same phenotypes as mutations deactivating these genes, because it might interfere with the protein function or disrupt the balanced stoichiometry of its multiprotein complex [65]. It is noteworthy in this context that the levels of DP71f expression in our study were exceedingly low, underscoring the stringent regulation of its expression levels.

We also found that Dp71f knockout increases cell adhesion and reduces their ability to survive in no adhesion conditions, as shown by increased *anoikis*, which eliminates detached cells and prevents their re-attachment and uncontrolled growth [50]. This could indicate an adaptation in cell behaviour, where increased adhesion becomes crucial for survival. The altered adhesion in knockouts aligns with molecular finding that the DEGs between knockout and control cells exhibit enrichment in the ECM-receptor interaction pathway (11 genes showed downregulation in expression, while six genes were upregulated). *Anoikis* is regulated by integrin-mediated cell-ECM interactions [66] and Dp71f was found associated with the β1-integrin adhesion complex in various cells [36, 38]. However, in some studies, Dp71f depletion resulted in a decrease in the β1-integrin adhesion complex components and a failure in adhesion [36]. Thus, the effect of Dp71f on adhesion may be cell-specific, possibly because of the presence of distinct Dp71f interacting partners/accessory proteins.

Activation of the PI3K/Akt signalling pathway, and resultant apoptosis inhibition, may contribute to enhanced survival during serum starvation [67], a recognized tumour cell adaptation [68, 69], and to reduced etoposide sensitivity [70]. While 39 DEGs associated with this pathway were identified in knockout cells (Supplementary Table 1), statistical enrichment was not significant ($P = 0.245$). However, the PI3K/Akt pathway showed enrichment in DEGs between primary mesothelioma samples with low versus high Dp71f expression [5], and it is altered in the skeletal muscle of DMD patients [71]. Further analysis of the PI3K/Akt pathway in dystrophy seems warranted.

Many of the observed alterations could be linked to the profound metabolic impact of Dp71f knockout that we identified in the GSMM. This included the downregulation of glucose transport via membrane vesicle reaction (GLCter) corresponding with GLUT1 glucose transporter downregulation (Fig. 5), which indicates a diminished glucose uptake. Combined with the decreased glycolysis/gluconeogenesis pathway exemplified by the downregulated HEX1 reaction, responsible for converting glucose to glucose-6-phosphate [72], these suggest a significant impact on cellular glucose homeostasis and energy metabolism. Furthermore, the downregulation of GLU5Km and G5SDym reactions in the arginine and proline metabolism pathway indicate a potential glutamate levels disruption. Glutamate, the very important carbon sources in the TCA cycle, is central in metabolic processes influencing cell growth [73]. The downregulation of the tyrosine kinase in the transport reaction pathway agrees with aberrant cellular growth and resistance to therapy [74], as does the increased activity of SBPP1er reaction ($\log_2$FC = 5.234) in the sphingolipid metabolism pathway, also known to influence cell proliferation, survival, and apoptosis [75]. The upregulation of PSDm_hs in the mitochondrial glycerophospholipid metabolism pathway agrees with alterations in cell signalling, and apoptosis [76] by impacting phospholipid metabolism and membrane fluidity.

Expression of Dp71f did not significantly affect cell migration and invasion, despite knockout cells showing elevated levels of gelatinases known to promote tumour cell invasion [77]. This might be attributed to the increased expression of endogenous MMP inhibitors observed in knockout cells [78, 79], similar to findings in dystrophic muscles [80, 81]. Although RNAseq data did not reveal upregulation of MMP inhibitors, protein levels were not evaluated.

Our findings show that Dp71f knockout affects various aspects of cell function in sarcoma cells, including metabolism, calcium signalling, proliferation, cell adhesion, and responsiveness to chemotherapy. Loss of Dp71f expression could contribute to the lack of beneficial treatment effect of etoposide in subsets of Ewing sarcoma patients [82]. However, a limitation of this study

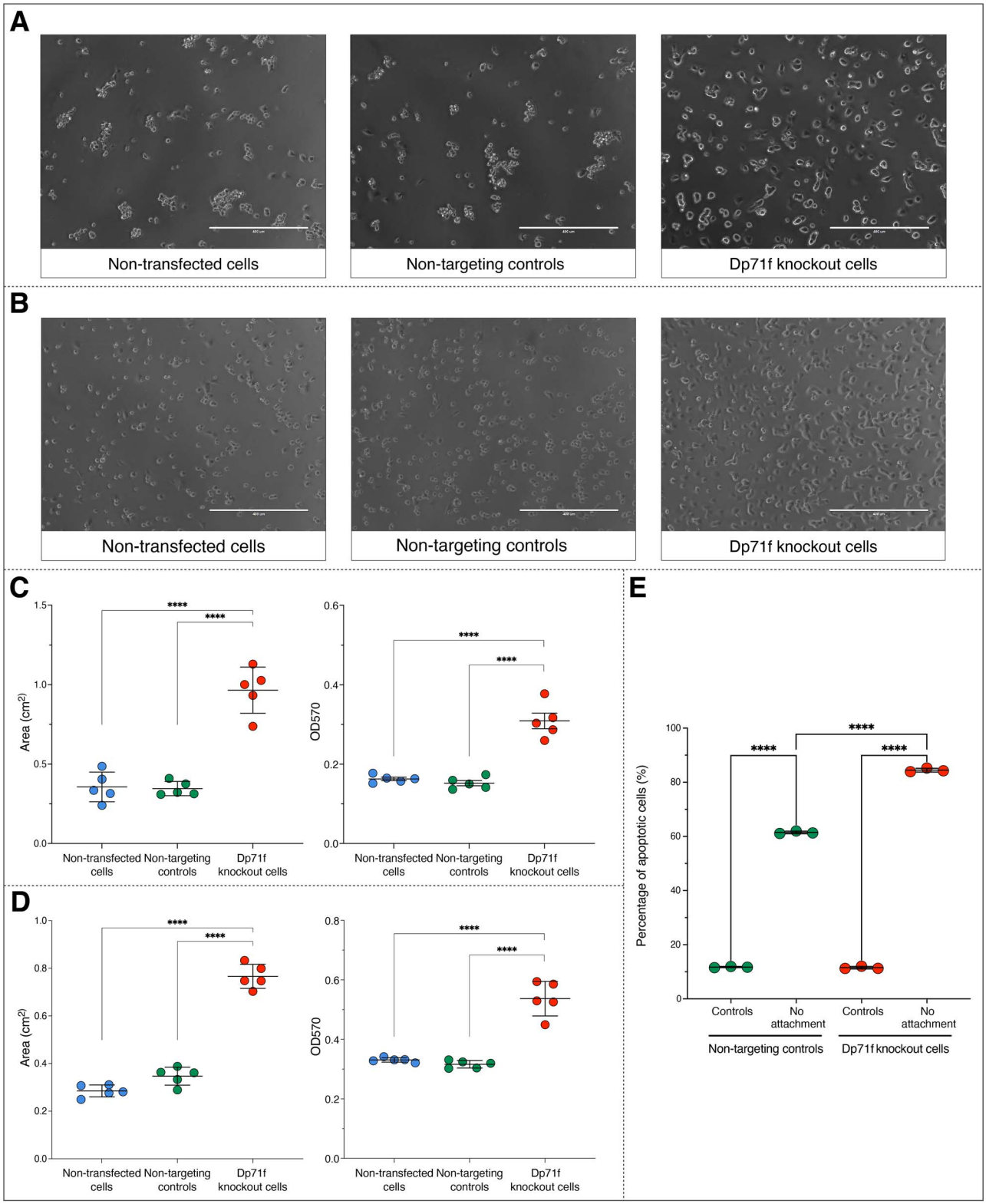

Figure 10. Cell adhesion and *anoikis* are increased in Dp71f knockout cells. Phase contrast microscopy images for the adhesion assay performed on non-coated (A) and Geltrex™-coated (B) plates. The area of stained cells in cm^2 (left) and the OD_{570} measurements of the solubilised crystal violet dye (right) for cells on non-coated (C) and Geltrex™-coated (D) plates. Data is presented as mean ± SD (n = 5 per group). (E) Percentage of apoptotic cells 48 h following culture in ultra-low attachment flasks compared to controls (n = 3 per group).

is the availability of only one cell line expressing exclusively this specific splice variant. While the role of Dp71f in cell proliferation aligns with literature data, the direction of changes evoked by this variant on other functions may be more cell-specific. The *DMD* gene, which has housekeeping characteristic [4], appears to encode a set of multifunctional molecular tools. While some

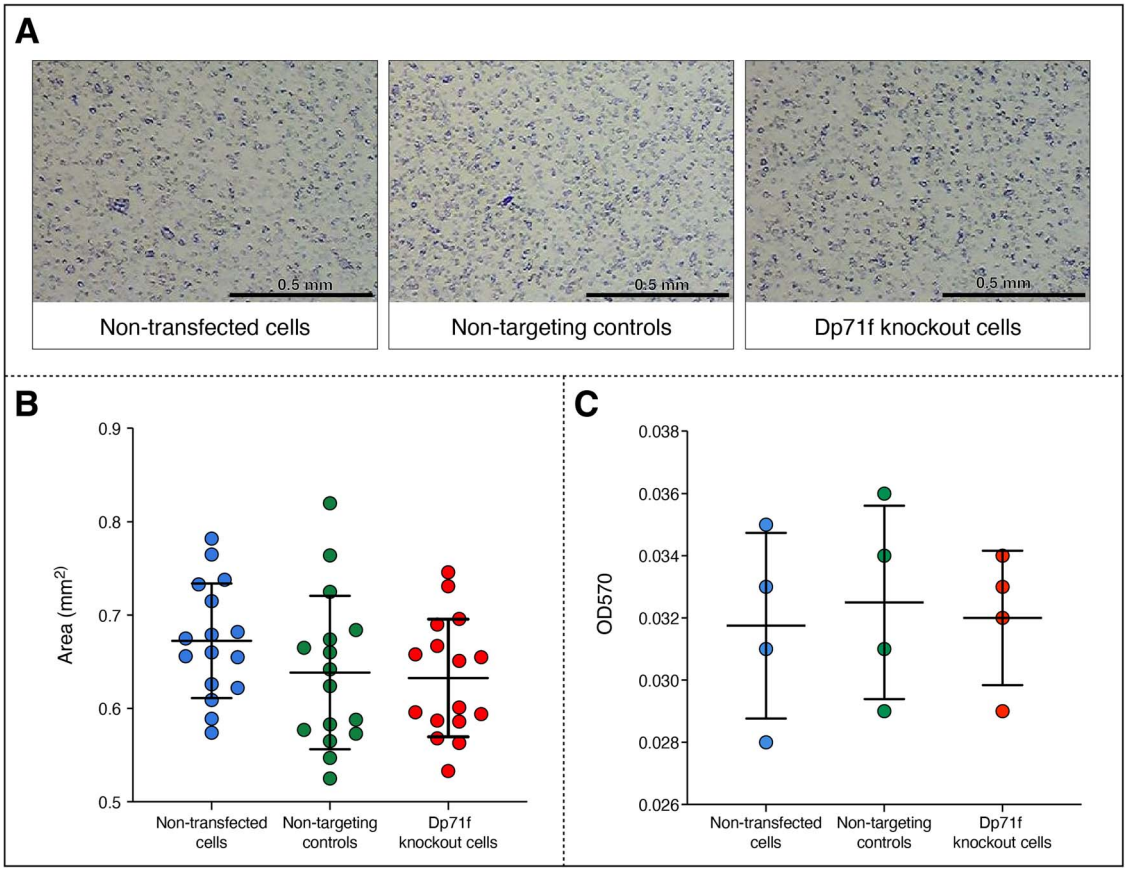

Figure 11. Cell migration is unaltered in Dp71f knockout cells in the Boyden chamber assay. (A) Digital images of the stained migrating cells at the lower surface of transwell inserts. (B) Area of cells in mm^2. Data is presented as mean ± SD (4 transwell inserts per group and 4 random sites per insert). (C) OD_{570} measurements of solubilised crystal violet (n = 4 per group).

of these tools serve similar functions across different cell types, others appear highly specialised and tailored to specific cells.

Interestingly, Dp71f was found to regulate these key cell functions, despite its protein level being very low, beyond the detection levels of a standard Western blot with two (MANDRA1 and MANDRA11) out of three highly specific antibodies. This parallels the situation where dystrophic abnormalities were identified in myoblasts and lymphoblasts [59], which express the full-length *DMD* gene transcript but have little or no detectable full-length dystrophin protein [83–87]. Yet, its loss triggers major abnormalities encompassing defects in proliferation [9, 10], migration [11], chemotaxis [9], differentiation and fusion [9, 88–90], energy metabolism [13] as well as impaired purinergic and cellular calcium responses [13, 91, 92]. These effects are likely to be due to the tightly spatiotemporally controlled expression of very small amounts of dystrophin protein (as shown here), but some regulatory function evoked by the dystrophin transcript(s) cannot be excluded. Importantly, no dystrophin expression can be considered as irrelevant or "illegitimate".

Our study highlights the significance of identifying the Dp71 splice variants expressed to understand the phenotypic outcomes. Given that Dp71f plays essential roles in cellular metabolism, adhesion and calcium homeostasis, processes commonly dysregulated in tumours, this work adds valuable insights to the growing body of evidence illustrating the diverse functions of *DMD* gene transcripts across various malignancies and this renders this variant a compelling target for future investigations.

Materials and methods

Public gene and protein expression datasets

The DepMap portal was interrogated for tumour cell lines with *DMD* gene expression. The datasets "Expression Public 23Q2" and "CCLE_expression_transcripts_expected_count" were used to examine RNA expression at the gene and transcript level, respectively. The dataset "Proteomics" was used to evaluate mass-spectrometry-based protein expression data in tumour cell lines.

Cell culture

The human Ewing sarcoma cell line A673 was maintained in Dulbecco's modified Eagle medium (DMEM) with high glucose and sodium pyruvate (Gibco™) supplemented with 10% foetal bovine serum (Gibco™), 2 mM L-glutamine, 100 U/ml penicillin and 100 μg/ml streptomycin (Fisher Scientific, Loughborough, UK). Cultured cells were kept in a humidified incubator at 37°C and 5% CO_2.

Generation of *DMD* gene knockout A673 cells

The CHOPCHOP tool (https://chopchop.rc.fas.harvard.edu) was used to design a single guide RNA (sgRNA) that targets exon 69 (CATGGTGGAATATTGCACTC). The sgRNA was made by GenScript and cloned in an All-in-One plasmid vector (eSpCas9-2A-Puro (PX459) V2.0) encoding a puromycin resistance gene. Non-targeting controls were generated using a plasmid vector encoding a sgRNA that does not target any known human

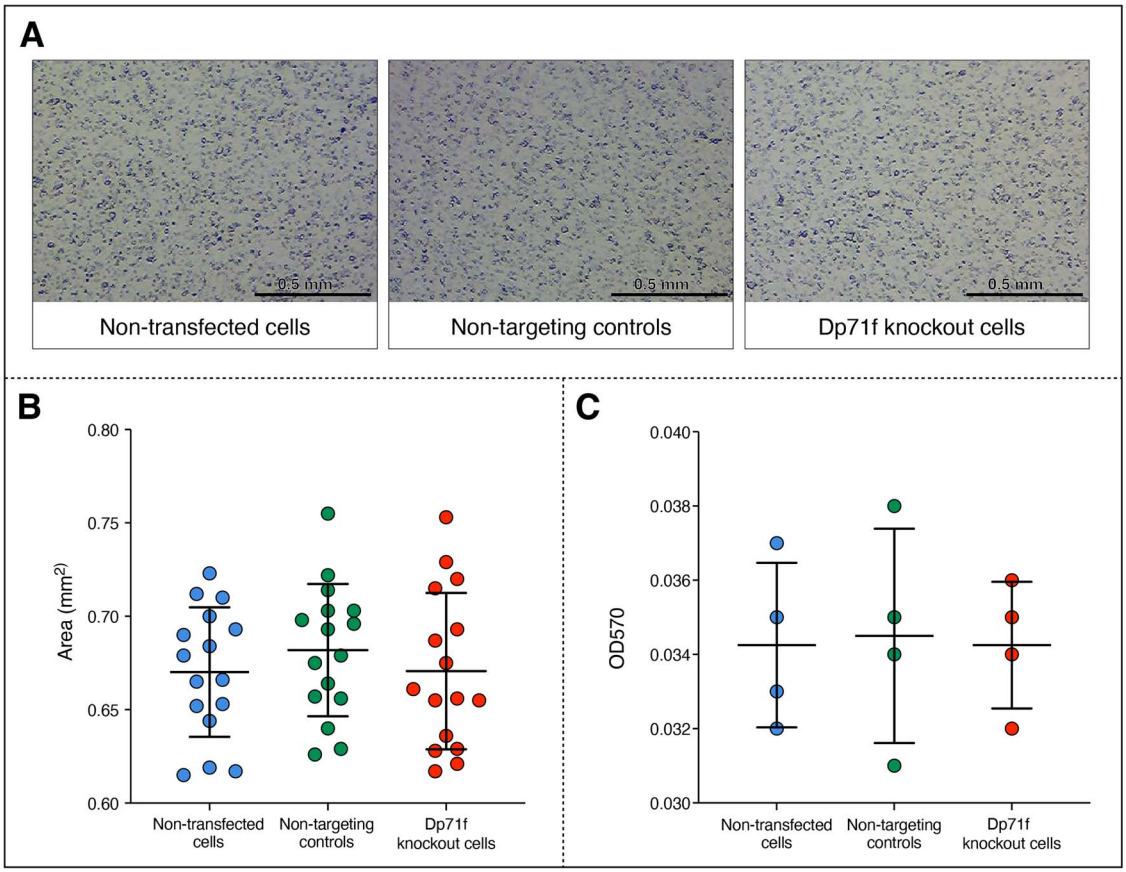

Figure 12. Cell invasion is unaltered in Dp71f knockout cells in the Boyden chamber assay. (A) Digital images of the stained invading cells at lower surface of transwell inserts. (B) Area of cells in mm^2. Data is presented as mean ± SD (4 transwell inserts per group and 4 random sites per insert). (C) OD_{570} measurements of solubilised crystal violet (n = 4 per group).

gene (GCCCCGCCGCCCTCCCCTCC). The cells were transfected with 2500 ng of plasmid DNA using the Lipofectamine™ 3000 transfection reagent (Thermo Scientific™) according to the manufacturer's instructions. Transfected cells were selected by exposure to 3 μg/ml of puromycin (Sigma) for five days. After that, single cells were isolated to generate clonal lines.

Validation of *DMD* gene knockout

Genomic DNA (gDNA) was extracted from single cell-derived clones using the DNeasy® Blood and Tissue DNA extraction kit (Qiagen). gDNA was amplified using the OneTaq® Quick-Load® 2X master mix (New England Biolabs) and 400 nM of primers. The NCBI primer designing tool (https://blast.ncbi.nlm.nih.gov/Blast.cgi) was used to design primers that span the target site of the sgRNA (Table 2; primer pair 1).

Thermal cycling conditions consisted of an initial denaturation step at 94°C for 30 s, followed by 35 cycles of 94°C for 15 s, 60°C for 30 s and 68°C for 30 s. PCR products were purified using the QIAquick PCR Purification Kit (Qiagen) and were Sanger sequenced (Azenta Life Sciences). Ab1 files were read by the FinchTV chromatogram viewer (https://digitalworldbiology.com/finchtv). The knockout status of single cell-derived clones was visually inspected by comparing Sanger traces with the wildtype reference sequence.

RNA extraction

Total RNA was extracted using the RNeasy Plus Universal Mini kit (Qiagen) and gDNA was removed using the RapidOut DNA removal kit (Thermo Scientific™). RNA concentration and purity were established using the Nanodrop ND-1000 spectrophotometer. A A260/A280 ratio of ~2.0, and a A260/A230 ration of 2.0–2.2 were considered acceptable.

RNA sequencing and data analysis

The libraries were sequenced with NovaSeq 6000 at Theragen Bio, resulting in about ~15 Gbp of total bases for each library. Raw sequencing data (FASTQ files) were processed using nf-core/rnaseq (version 3.12.0 available at DOI 10.5281/zenodo.1400710) of the nf-core collection of workflows [93] with default parameters. Data were assessed for quality and aligned to the human reference genome, Ensembl GRCh38 v109. Differential expression analysis of gene counts between groups was performed with the R package EdgeR v3.38.4 [94]. Genes were deemed statistically significant with EdgeR's quasi-likelihood F-tests (QLF) tests for given contrasts: non-targeting control vs non-transfected cells, knockout vs non-transfected cells, and knockout vs non-targeting control. P-values were adjusted for multiple testing using the Benjamini-Hochberg method to control the false discovery rate (FDR). Gene with an FDR-adjusted *P*-value < 0.001 and an absolute Log_2 Fold Change (FC) value ≥ 2 were considered to be differentially expressed. The EnrichR tool [95] was used to identify the Kyoto Encyclopaedia of Genes and Genomes (KEGG) pathways enriched in the differentially expressed genes (DEGs). The quantitative exon expression levels of *DMD* transcripts were determined using featureCounts v2.0.6 by counting aligned reads that overlapped with exon regions.

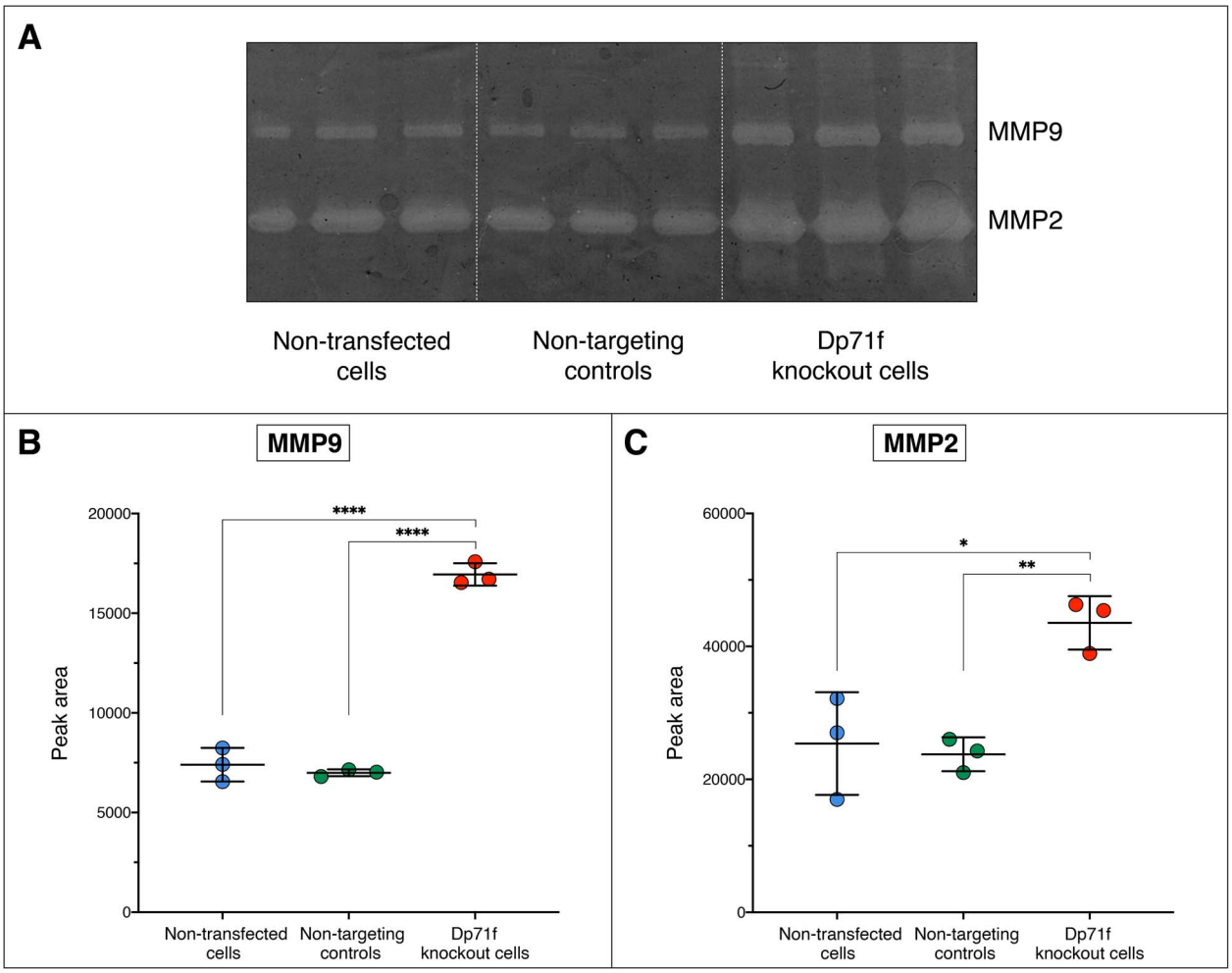

Figure 13. Release of active gelatinases is increased in Dp71f knockout cells. (A) A greyscale image of the 10% polyacrylamide gels containing 1 mg/ml gelatin showing gelatinolytic activity of MMP9 and MMP2 visible as transparent bands in the dark background. Densitometric quantification of (B) MMP9 and (C) MMP2 bands using ImageJ. Data is presented as mean ± SD (n = 3 per group).

Table 2. Primer sequences used in PCR experiments and their source.

Primer pair	Primer Name	Primer sequence (5′ → 3′)	Annealing temperature (°C)	Source
1	Intron 68 (F)	GTCTGTCGCTCCTGGAAGTT	60	NCBI primer designing tool
	Intron 69 (R)	TAAGATCGCCCCACACAACC		
2	Dp427m exon 1 (F)	TCGCTGCCTTGATATACACTTTTCA	62	[107]
	Dp427m exon 3 (R)	GGTTCTCAATATGCTGCTTCCCA		
3	Dp71 exon 1 (F)	CATGAGGGAACAGCTCAAAGGC	62	[107]
	Dp71 exon 64 (R)	CAGTCTTCGGAGTTTCATGGCA		
4	DMD exon 67	TCCGGAGCTGCTTCCAATTT	57	NCBI primer designing tool
	DMD exon 72	ATCGTGTGAAAGCTGAGGGG		
5	DMD exon 76	CTTCGGACTCCATGGTGAGG	55	NCBI primer designing tool
	DMD exon 79	TCACGCCAAAAGGATGCAAA		
6	DMD exon 68 (F)	CTGCTGCAGAAACTGCCAAG	60	NCBI primer designing tool
	DMD exon 69-70 (R)	CTCCTGATGTAGTCGGAGTGC		

Sashimi plots illustrating the findings were generated with IGV v2.12.3.

The genome-scale metabolic model

Genome-scale metabolic model (GSMM) was reconstructed using the extensively curated Human-GEM model version 1.17.0 [96], using our established methodology ensuring accuracy and relevance to individual cell samples [96]. Dead-end metabolites and reactions were removed, as they do not carry any fluxes and are not part of metabolic pathways. The upper and lower bounds of the reactions were constrained with transcriptomics data, thus tailoring the models to the specific expression profiles of each sample. To evaluate the metabolic alterations, we employed Flux Variability Analysis (FVA) with biomass as an objective function. The resulting sample-specific GSMMs were then analysed for flux rates using FVA, and to quantify and compare these alterations we

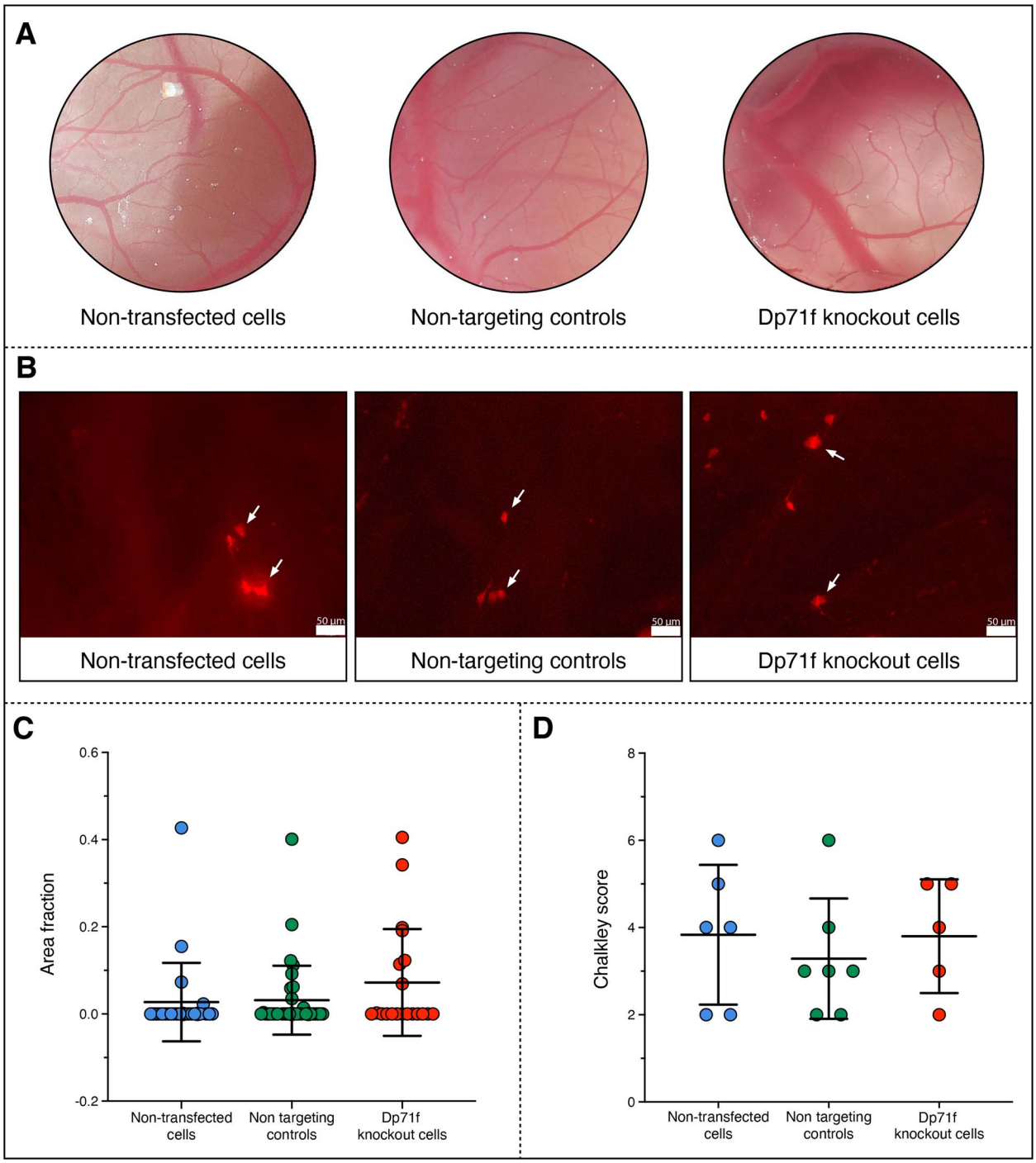

Figure 14. Cell invasive and angiogenic capacities are unaltered in Dp71f knockout cells in the CAM assay *in vivo*. (A) Representative images of the CAM membranes at the end of the assay. (B) Digital images of the fluorescently labelled cells (red, indicated by the white arrows) that have migrated from the seeding site and into the CAM membranes. (C) Area fraction measurements representing the proportion of images occupied by fluorescently labelled cells, indicating invasiveness. Data presented as mean ± SD (n = 4–7 membranes per group and 5 random sites per membrane). (D) Chalkley score values providing a measure of the extent of angiogenesis in the membranes. (n = 5–7 per group).

computed the FC of flux rates between the knockout and control cells.

PCR and gel electrophoresis

cDNA was synthesised from 2 μg of total RNA using the High-Capacity RNA-to-cDNA™ Kit (Applied Biosystems™). Human skeletal muscle total RNA (Takara Bio) was used as a positive control for *DMD* expression. cDNA was amplified using the OneTaq® Quick-Load® 2X master mix (New England Biolabs) and 400 nM of primers (Table 1). The thermal cycling conditions and annealing temperatures listed in Table 1 were used. PCR products were resolved in a 2% UltraPure™ agarose gel (Thermo Scientific™) stained with SYBR™ Safe DNA gel stain (Invitrogen™). A 4% agarose gel was used for the PCR products of primer pairs 4 and 5.

Protein extraction

The cells were harvested and lysed in ice-cold RIPA Buffer (Thermo Scientific™) containing cOmplete™ ULTRA tablets, mini,

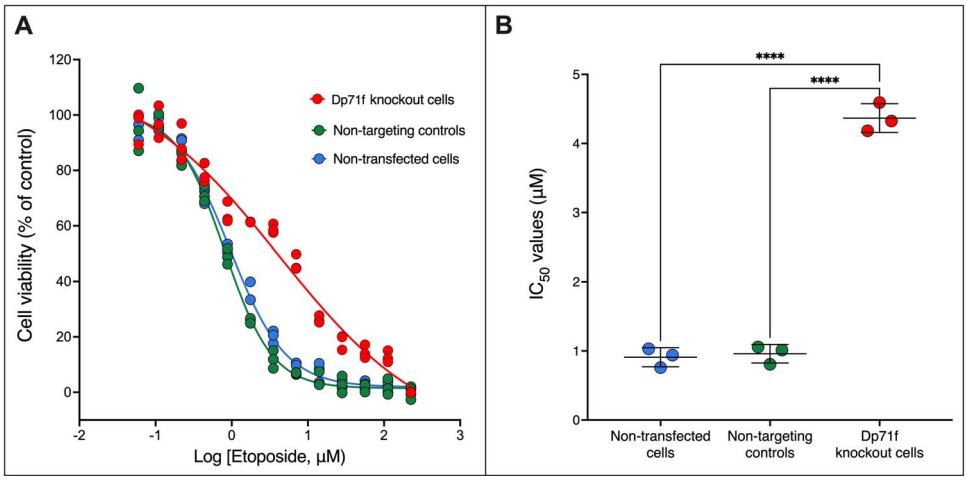

Figure 15. Loss of Dp71f decreases sensitivity to etoposide. (A). Sigmoidal dose–response curves generated by nonlinear regression (n = 3 for each etoposide concentration). (B) Etoposide IC_{50} values calculated from three independent experiments. Data is presented as mean ± SD.

EDTA-free, EASYpack protease inhibitor cocktail (Roche). Mouse cerebellum was used as a positive control for Dp71 expression. The cerebellum tissue was lysed in ice-cold RIPA Buffer with protease inhibitors and homogenised by passing through a 25G needle 20 times. After incubation at 4°C for 30 min on a bench rocker, the cell and tissue lysates were centrifuged at 16 000 g for 20 min to pellet the debris. The protein concentrations of lysates were determined using the Pierce™ BCA Protein Assay Kit (Thermo Scientific™) using manufacturer's instructions.

Western blotting

Lysates containing 60 μg of protein were mixed 1:1 with Novex™ Tris-Glycine SDS sample buffer (Invitrogen™) with 5% β-mercaptoethanol (Sigma) and heat denatured at 95°C for five minutes (except for GLUT1 detection). Protein samples and protein size markers (Precision Plus Protein™ Kaleidoscope™ Prestained Protein Standards ladder; BioRad) were loaded into the wells of an SDS-PAGE gel composed of a 10% resolving gel and a 4% stacking gel. Following electrophoresis, the proteins were transferred to a PDVF transfer membrane (Amersham™ Hybond®). Protein transfer was assessed by reversibly staining the membrane with Ponceau S Staining Solution (Thermo Fisher Scientific™) and staining the post-transfer gel with Coomassie Brilliant Blue (CBB) (NIH, Bethesda, MD, USA). The membranes were blocked with 5% non-fat milk in TBST (15.2 mM Tris–HCl, 4.62 mM Tris base, 150 mM NaCl and 0.01% Tween-20) and incubated at 4°C overnight with a specific primary antibody (Table 3). The membranes were washed 4×10 min with TBST and incubated with a horseradish peroxidase-conjugated secondary antibody (Table 3) at room temperature for an hour. The protein bands were detected using the chemiluminescent substrate, Luminata Crescendo (Millipore) and the ChemiDoc™ XRS+ System (BioRad). All experiments were repeated at least three times. The band intensities of GLUT1 were normalized to the total protein intensities in the corresponding CBB-stained lanes and quantified using the integrated density measurement function of ImageJ software [97]. Statistical analyses on the average densitometric values from three repeats were performed as described below.

Calcium assay

Cells were seeded at a density of 300 000 cells on glass coverslips in a 24-well plate. After 48 h, coverslips were incubated for an hour at room temperature protected from the light in a buffer (133 mM NaCl, 3 mM KCl, 2.24 mM $CaCl_2$, 1.2 mM NaH_2PO_4, 1 mM $MgCl_2$, 10 mM HEPES, 10 mM D-glucose, pH 7.3) containing 4 μM Fluo-4, AM (Invitrogen™), which was made up fresh from stock. Coverslips were transferred to a perfusion chamber mounted to the Zeiss LSM 510 PASCAL Axioskop 2 confocal microscope and were kept in a continuous flow of buffer using a multitap system that allowed rapid turnover of solutions. Labelled cells were excited with the 488 nm argon laser and emitted fluorescence was collected at 510–580 nm. Adenosine 5′-triphosphate (ATP, Sigma; 100 μM) was applied by perfusion over the coverslips for 30 s. Confocal images were captured using an Achroplan 20×/0.50 WPh2 water immersion lens at 30 s intervals. Time lapse images were imported into the ImageJ software (https://imagej.nih.gov/ij/). A graph for fluorescence over time was generated using (Image > Stacks > Plot Z-axis Profile) to identify the frame at which the fluorescence intensity peaks and evaluate the change in fluorescence compared to baseline before ATP addition. The proportion of each image occupied by fluorescent cells was measured and the percentage change of fluorescence from baseline was calculated as follows: (fluorescence after addition of ATP—fluorescence at baseline)/fluorescence at baseline) × 100.

Proliferation assays

Cell proliferation was evaluated using the PrestoBlue™ cell viability reagent (Invitrogen™) and crystal violet staining. Under normal serum conditions, cells were seeded at 5000 cells per well in a 96-well plate and incubated for 72 h. To examine proliferation in low serum conditions, cells were seeded at 10 000 cells per well in a 96-well plate in their usual media for 24 h, and then the media were changed to 2% FBS-containing media for 48 h. After incubation, digital images were obtained with a 10× objective using the Leica DMi1 inverted microscope equipped with the high-resolution digital camera Leica MC170 HD (Leica Microsystems). The PrestoBlue™ fluorescence was measured at 560 nm using the SpectraMax® i3× multi-Mode microplate reader (Molecular Devices). For the crystal violet assay, the protocol described in [98] was used. Digital images of the stained plates were imported into ImageJ to measure the area of stained cells in each well. The crystal violet dye was then solubilised in methanol (Fisher BioReagents™) and the optical density measured at 570 nm (OD_{570}) using the SpectraMax® i3× microplate reader.

Table 3. Primary and secondary antibodies used for western blotting.

Antibody	Dilution (final concentration)	Supplier
MANDRA1 (7A10)—mouse anti-dystrophin (exon 77)	1:100 (1.3 ug/ml)	Wolfson Centre for Inherited Neuromuscular Disease
MANEX7374J—mouse anti-dystrophin (exon 73/74)	1:100 (~1.2 μg/ml)	Wolfson Centre for Inherited Neuromuscular Disease
MANDRA11—mouse anti-dystrophin (exon 75)	1:100 (1.14 μg/ml)	Wolfson Centre for Inherited Neuromuscular Disease
Rabbit anti-GLUT1	1:10000 (0.02 μg/ml)	Abcam (ab115730)
Anti-mouse-HRP	1:10000 (0.1 ug/ml)	Sigma (A4416)
Anti-rabbit-HRP	1:20000 (0.5 ug/ml)	Sigma (A0545)

Colony formation assay

Cells were seeded at a concentration of 1000 cells per well in a six-well plate and media were changed every 2–3 days. After two weeks, colonies were fixed in 10% formalin (Sigma) and stained with 0.5% crystal violet solution. Digital images of the stained plates were collected and the number of colonies in each well was determined using ImageJ.

Adhesion assay

Cells were seeded at 200 000 cells per well in a non-ECM coated 24-well plate or a 24-well plate coated with Geltrex™ LDEV-free reduced growth factor basement membrane matrix (Thermo Scientific™). Cells were incubated for two hours and were then imaged with a 10× objective using the EVOS® FL Auto Cell Imaging System (Invitrogen™). Cells were washed with PBS to remove nonadherent cells and were fixed with 10% formalin and stained with 0.5% crystal violet. Digital images of the stained plates were imported into ImageJ to measure the area of stained cells in each well. The OD_{570} of the methanol-solubilised crystal violet was measured using the SpectraMax® i3x microplate reader.

Transwell migration and invasion assays

The protocol described in [99] was used. Cultured cells were serum-starved for 24 h prior to the experiment by replacing their usual media with 1% FBS-containing media. On the day of the experiment, 20 000 cells were added to the top compartment of a transwell insert (pore size 8 μm; Sarstedt) placed in a 24-well plate containing media with 5% FBS. Transwell inserts with 50 μl of the Geltrex™ matrix coating were used for the invasion assay. Cells were then incubated for 6 h for the migration assay and 18 h for the invasion assay. Migrating or invading cells on the lower surface of the Transwell insert were fixed using 10% formalin and stained with 0.5% crystal violet solution. Digital images of the stained cells were obtained with a 2.0× magnification using the Stemi 305 microscope (ZEISS). For each transwell insert, images were obtained for four randomly selected sites. Images were imported into ImageJ to measure the area of stained cells. Area measurements were analysed in IBM SPSS® Statistics using a univariate linear mixed model with Condition as a fixed factor (non-transfected cells, non-targeting controls, and knockout cells) and Transwell replicate as a random factor to account for the four different area measurements for each transwell insert. A Tukey's multiple comparisons test was used to compare are measurements between the three conditions. The OD_{570} of the methanol-solubilised crystal violet was measured using the SpectraMax® i3× microplate reader.

Wound healing assay

Cells were cultured in a 6-well plate until they formed a confluent monolayer. Subsequently, the serum-containing media were removed, and cells were washed with PBS. Serum-free media were added, and cells were incubated for a further 24 h to suppress the ability of cells to proliferate and minimise the effect of cell proliferation on wound closure. A sterile P20 pipette tip was used to create a wound and cells were washed with PBS to remove detached cells and debris. Serum-free media were subsequently added, and digital images were obtained with a 10× objective using the Leica DMi1 inverted microscope and Leica MC170 HD camera (Leica Microsystems).

Gelatin zymography

Cells were cultured to 70% confluency and were then washed with PBS and continued to grow in FBS-free media for 48 h. The conditioned media were centrifuged to eliminate dead cells and were concentrated using Pierce™ Protein Concentrators, PES, 10 K MWCO (Thermo Scientific™) at 3000 g for 20 min. For each sample, a volume containing 5ug of protein was mixed 1:1 with Novex™ Tris-Glycine SDS sample buffer (Invitrogen™), and proteins were resolved in a 10% polyacrylamide gel containing 1 mg/ml gelatin (Sigma). Gels were washed three times in 2.5% Triton X-100 and were then incubated in the developing buffer (50 mM Tris–HCl, 10 mM $CaCl_2$; pH 7.5) for 18 h. Gels were stained with Coomassie brilliant blue G, and the gelatinolytic activity was identified as transparent bands in the blue-stained background. Quantification of MMP9 and MMP2 bands was determined by densitometry using ImageJ as described in [100].

Cell apoptosis and anoikis assays

To evaluate the effects of serum starvation on cell apoptosis, 1×10^6 cells were cultured in serum-free media in a 6-well plate for 48 h. To examine anoikis, 1×10^6 cells were seeded in ultra-low attachment plates (Corning™) for 48 h. Control cells maintained in their usual FBS-containing media under standard culture conditions were also incubated for the same period of time. Next, the Annexin V–CF Blue/propidium iodide (PI) apoptosis detection kit (Abcam) was used according to the manufacturer's instructions and cells were immediately analysed using CytoFLEX S (Beckman Coulter, USA).

Determination of cell viability following etoposide exposure

Cells were seeded at a density of 5000 cells in a 96-well plate. After 24 h, cells were treated with etoposide (Sigma) prepared in dimethylsulfoxide (DMSO; Sigma). Etoposide concentrations ranged from 0.06 μM to 225.28 μM. Each measurement was performed in triplicates. Untreated cells, cells treated with corresponding concentrations of DMSO, and media only controls were included. After 48 h, cell viability was determined using the PrestoBlue™ reagent, and fluorescence was measured at 560 nm using the POLARstar Optima plate reader (BMG Labtech). Sigmoidal dose–response curves were generated by nonlinear

regression in GraphPad Prism and were used to calculate the half maximal inhibitory concentration (IC_{50}) values.

The Chick Chorioallantoic membrane (CAM) assay

The CAM assay is widely used as an in vivo model to evaluate angiogenesis [101] and tumour cell invasion and metastasis [102–105]. All procedures were performed with prior local and Home Office ethical approval and in accordance with the guidelines and regulations stated in the Animals (Scientific Procedures) Act 1986. In these sets of studies, a UK Personal Project License (PPL) was not needed as the eggs were used until embryonic day (ED) 10 when the experimental study ended. Briefly, fertilised hens (*Gallus gallus* domesticus) eggs (Medeggs, Henry Stewart & Co., Lincolnshire) were incubated at 37°C in a humidified (60%) incubator with rotation (Hatchmaster incubator, Brinsea, UK). At ED3 of incubation, 3 mL of albumin were removed from the egg and returned to the incubator [106]. At ED7, a small window (approximately 1 cm^2) was created, and a sterile cloning ring (5 mm in diameter) was placed on the membrane. A673 cells (8×10^6) were stained with 25 μM of CellTracker™ Red CMTPX Dye (Invitrogen™) for 45 min. Cells were then centrifuged at 500 g for five minutes and resuspended in serum-free media. 100 μl of cell suspension containing 5×10^4 cells were injected into the cloning ring on the CAM membrane. The window was sealed with sterile parafilm, and the eggs were incubated for a further 72 h. Digital images of the CAM membranes were collected, and angiogenesis was quantified using a Chalkley graticule in the eyepiece of the dissecting microscope. Chalkley score values provide a measure of the extent of angiogenesis or blood vessel formation in the membranes. CAM membranes were then fixed in 4% formaldehyde solution, and fluorescence microscope images of five random fields for each CAM membrane were captured to visualise cells that had migrated into the CAM from the sterile cloning ring seeding site. The area fraction measurements were calculated using ImageJ to determine the proportion of each image occupied by stained cells.

Statistical analysis

Data were tested for normality using a Shapiro–Wilk test in GraphPad Prism. Normally distributed data were analysed using an unpaired t-test or an ordinary one-way Analysis of Variance (ANOVA) and Tukey's multiple comparisons test (when the groups had equal variances), while non-normally distributed data were analysed using a Mann–Whitney test or Kruskal Willis and Dunn's multiple comparisons tests. Asterisks indicate the level of significance: $^*P < 0.05$, $^{**}P < 0.01$, $^{***}P < 0.001$ and $^{****}P < 0.0001$.

Acknowledgements

The authors gratefully acknowledge support from Richard Oreffo in performing the CAM assay, Helen Filmore for providing Etoposide and advice on the chemosensitivity assay. Funding from the University of Portsmouth (under the Strategic PhD studentships scheme) is gratefully acknowledged. The work described in this article was supported by the COST Action CA21130 "P2X receptors as a therapeutic opportunity (PRESTO).

Supplementary data

Supplementary data is available at *HMG Journal* online.

Conflict of interest statement. Authors declare no conflict of interest.

Funding

None declared.

References

1. Duan D, Goemans N, Takeda S. *et al.* Duchenne muscular dystrophy. *Nat Rev Dis Primers* 2021;**7**:1–19.
2. Massouridès E, Polentes J, Mangeot PE. *et al.* Dp412e: a novel human embryonic dystrophin isoform induced by BMP4 in early differentiated cells. *Skelet Muscle* 2015;**5**:1–18.
3. Mournetas V, Massouridès E, Dupont JB. *et al.* Myogenesis modelled by human pluripotent stem cells: a multi-omic study of Duchenne myopathy early onset. *J Cachexia Sarcopenia Muscle* 2021;**12**:209–232.
4. Alnassar N, Borczyk M, Tsagkogeorga G. *et al.* Downregulation of dystrophin expression occurs across diverse Tumors, correlates with the age of onset, staging and reduced survival of patients. *Cancers (Basel)* 2023;**15**:1378.
5. Alnassar N, Derry JMJ, Banna GL. *et al.* Differential expression of DMD transcripts as a novel prognostic biomarker in histologically diverse mesotheliomas. *Transl Lung Cancer Res* 2024;**13**:733–748.
6. Jones L, Naidoo M, Machado LR. *et al.* The Duchenne muscular dystrophy gene and cancer. *Cell Oncol* 2021;**44**:19–32.
7. Broomfield J, Hill M, Guglieri M. *et al.* Life expectancy in Duchenne muscular dystrophy. *Neurology* 2021;**97**:e2304–e2314.
8. Farea M, Rani AQM, Maeta K. *et al.* Dystrophin Dp71ab is monoclonally expressed in human satellite cells and enhances proliferation of myoblast cells. *Sci Rep* 2020;**10**:1–8.
9. Gosselin MR, Mournetas V, Borczyk M. *et al.* Loss of full-length dystrophin expression results in major cell- autonomous abnormalities in proliferating myoblasts. *elife* 2022;**11**:e75521.
10. Melone MA, Peluso G, Petillo O. *et al.* Defective growth in vitro of Duchenne muscular dystrophy myoblasts: the molecular and biochemical basis. *J Cell Biochem* 2000;**76**:118–132.
11. Witkowski JA, Dubowitz V. Duchenne muscular dystrophy: studies of cell motility in vitro. *J Cell Sci* 1985;**76**:225–234.
12. Mareedu S, Million ED, Duan D. *et al.* Abnormal calcium handling in Duchenne muscular dystrophy: mechanisms and potential therapies. *Front Physiol* 2021;**12**:1–19.
13. Onopiuk M, Brutkowski W, Young C. *et al.* Store-operated calcium entry contributes to abnormal Ca2+ signalling in dystrophic mdx mouse myoblasts. *Arch Biochem Biophys* 2015;**569**:1–9.
14. Zabłocka B, Górecki DC, Zabłocki K. Disrupted calcium homeostasis in duchenne muscular dystrophy: a common mechanism behind diverse consequences. *Int J Mol Sci* 2021;**22**:11040.
15. Muntoni F, Torelli S, Ferlini A. Dystrophin and mutations: one gene, several proteins, multiple phenotypes. *Lancet Neurol* 2003;**2**:731–740.
16. Lederfein D, Yaffe D, Nudel U. A housekeeping type promoter, located in the 3′ region of the Duchenne muscular dystrophy gene, controls the expression of Dp71, a major product of the gene. *Hum Mol Genet* 1993;**2**:1883–1888.
17. Wang Y, Marino-enriquez A, Bennett RR. *et al.* Dystrophin is a tumor suppressor in human cancers with myogenic programs. *Nat Genet* 2014;**46**:601–606.

18. Mauduit O, Delcroix V, Lesluyes T. *et al.* Recurrent DMD deletions highlight specific role of Dp71 isoform in soft-tissue sarcomas. *Cancers (Basel)* 2019;**11**:922.
19. Tan S, Tan S, Chen Z. *et al.* Knocking down Dp71 expression in A549 cells reduces its malignancy in vivo and in vitro. *Cancer Investig* 2016;**34**:16–25.
20. Ruggieri S, De Giorgis M, Annese T. *et al.* Dp71 expression in human glioblastoma. *Int J Mol Sci* 2019;**20**:7–10.
21. Tan S, Tan J, Tan S. *et al.* Decreased Dp71 expression is associated with gastric adenocarcinoma prognosis. *Oncotarget* 2016;**7**:53702–53711.
22. Naidoo M, Jones L, Conboy B. *et al.* Duchenne muscular dystrophy gene expression is an independent prognostic marker for IDH mutant low-grade glioma. *Sci Rep* 2022;**12**:1–14.
23. Naidoo M, Anthony K. Dystrophin Dp71 and the Neuropathophysiology of Duchenne muscular dystrophy. *Mol Neurobiol* 2020;**57**:1748–1767.
24. Austin RC, Howard PL, D'souza VN. *et al.* Cloning and characterization of alternatively spliced isoforms of Dp71. *Hum Mol Genet* 1995;**4**:1475–1483.
25. Rau F, Lainé J, Ramanoudjame L. *et al.* Abnormal splicing switch of DMD's penultimate exon compromises muscle fibre maintenance in myotonic dystrophy. *Nat Commun* 2015;**6**:7205.
26. Greener MJ, Sewry CA, Muntoni F. *et al.* The 3′-untranslated region of the dystrophin gene - conservation and consequences of loss. *Eur J Hum Genet* 2002;**10**:413–420.
27. Aragón J, González-Reyes M, Romo-Yáñez J. *et al.* Dystrophin Dp71 isoforms are differentially expressed in the mouse brain and retina: report of new alternative splicing and a novel nomenclature for Dp71 isoforms. *Mol Neurobiol* 2018;**55**:1376–1386.
28. González-Ramírez R, Morales-Lázaro SL, Tapia-Ramírez V. *et al.* Nuclear and nuclear envelope localization of dystrophin Dp71 and dystrophin-associated proteins (DAPs) in the C2C12 muscle cells: DAPs nuclear localization is modulated during myogenesis. *J Cell Biochem* 2008;**105**:735–745.
29. Herrera-Salazar A, García-Villegas R, Aragón J. *et al.* Overexpression of mutant dystrophin Dp71δ2stimulates cell proliferation. *Neuroreport* 2016;**27**:6–11.
30. Marquez FG, Cisneros B, Garcia F. *et al.* Differential expression and subcellular distribution of dystrophin Dp71 isoforms during differentiation process. *Neuroscience* 2003;**118**:957–966.
31. Nishida A, Yasuno S, Takeuchi A. *et al.* HEK293 cells express dystrophin Dp71 with nucleus-specific localization of Dp71ab. *Histochem Cell Biol* 2016;**146**:301–309.
32. Shaw G, Morse S, Ararat M. *et al.* Preferential transformation of human neuronal cells by human adenoviruses and the origin of HEK 293 cells. *FASEB J* 2002;**16**:869–871.
33. Fuentes-Mera L, Rodríguez-Muñoz R, González-Ramírez R. *et al.* Characterization of a novel Dp71 dystrophin-associated protein complex (DAPC) present in the nucleus of HeLa cells: members of the nuclear DAPC associate with the nuclear matrix. *Exp Cell Res* 2006;**312**:3023–3035.
34. Tadayoni R, Rendon A, Soria-Jasso LE. *et al.* Dystrophin Dp71: the smallest but multifunctional product of the duchenne muscular dystrophy gene. *Mol Neurobiol* 2012;**45**:43–60.
35. Villarreal-Silva M, Suárez-Sánchez R, Rodríguez-Muñoz R. *et al.* Dystrophin Dp71 is critical for stability of the DAPs in the nucleus of PC12 cells. *Neurochem Res* 2010;**35**:366–373.
36. Cerna J, Cerecedo D, Ortega A. *et al.* Dystrophin Dp71f associates with the β1-integrin adhesion complex to modulate PC12 cell adhesion. *J Mol Biol* 2006;**362**:954–965.
37. Enríquez-Aragón JA, Cerna-Cortés J, De León MB. *et al.* Dystrophin Dp71 in PC12 cell adhesion. *Neuroreport* 2005;**16**:235–238.
38. García-Tovar CG, Luna J, Mena R. *et al.* Dystrophin isoform Dp71 is present in lamellipodia and focal complexes in human astrocytoma cells U-373 MG. *Acta Histochem* 2002;**104**:245–254.
39. Calderilla-Barbosa L, Ortega A, Cisneros B. Phosphorylation of dystrophin Dp71d by Ca2+/calmodulin-dependent protein kinase II modulates the Dp71d nuclear localization in PC12 cells. *J Neurochem* 2006;**98**:713–722.
40. Rani AQM, Farea M, Maeta K. *et al.* Identification of the shortest splice variant of dp71, together with five known variants, in glioblastoma cells. *Biochem Biophys Res Commun* 2019;**508**:640–645.
41. Adorisio R, Mencarelli E, Cantarutti N. *et al.* Duchenne dilated cardiomyopathy: cardiac management from prevention to advanced cardiovascular therapies. *J Clin Med* 2020;**9**:1–18.
42. Gao QQ, McNally EM. The dystrophin complex: structure, function, and implications for therapy. *Compr Physiol* 2015;**5**:1223–1239.
43. Ramirez MP, Anderson MJM, Kelly MD. *et al.* Dystrophin missense mutations alter focal adhesion tension and mechanotransduction. *Proc Natl Acad Sci USA* 2022;**119**:1–8.
44. Winkler J, Abisoye-Ogunniyan A, Metcalf KJ. *et al.* Concepts of extracellular matrix remodelling in tumour progression and metastasis. *Nat Commun* 2020;**11**:1–19.
45. He X, Lee B, Jiang Y. Extracellular matrix in cancer progression and therapy. *Med Rev* 2022;**2**:125–139.
46. Wu L, Lian W, Zhao L. Calcium signaling in cancer progression and therapy. *FEBS J* 2021;**288**:6187–6205.
47. Griffin JL, Williams HJ, Sang E. *et al.* Metabolic profiling of genetic disorders: a multitissue 1H nuclear magnetic resonance spectroscopic and pattern recognition study into dystrophic tissue. *Anal Biochem* 2001;**293**:16–21.
48. Górecki DC. P2X7 purinoceptor as a therapeutic target in muscular dystrophies. *Curr Opin Pharmacol* 2019;**47**:40–45.
49. Capiod T. Cell proliferation, calcium influx and calcium channels. *Biochimie* 2011;**93**:2075–2079.
50. Taddei ML, Giannoni E, Fiaschi T. *et al.* Anoikis: an emerging hallmark in health and diseases. *J Pathol* 2012;**226**:380–393.
51. Young CNJ, Chira N, Róg J. *et al.* Sustained activation of P2X7 induces MMP-2-evoked cleavage and functional purinoceptor inhibition. *J Mol Cell Biol* 2018;**10**:229–242.
52. Li H, Mittal A, Makonchuk DY. *et al.* Matrix metalloproteinase-9 inhibition ameliorates pathogenesis and improves skeletal muscle regeneration in muscular dystrophy. *Hum Mol Genet* 2009;**18**:2584–2598.
53. Brennan B, Kirton L, Marec-Bérard P. *et al.* Comparison of two chemotherapy regimens in patients with newly diagnosed Ewing sarcoma (EE2012): an open-label, randomised, phase 3 trial. *Lancet* 2022;**400**:1513–1521.
54. Crawford GE, Faulkner JA, Crosbie RH. *et al.* Assembly of the dystrophin-associated protein complex does not require the dystrophin COOH-terminal domain. *J Cell Biol* 2000;**150**:1399–1410.
55. Shih JA, Folch A, Wong BL. Duchenne muscular dystrophy: the heart of the matter. *Curr Heart Fail Rep* 2020;**17**:57–66.
56. Burnstock G. Purine and purinergic receptors. *Brain Neurosci Adv* 2018;**2**:239821281881749.
57. Di Virgilio F, Adinolfi E. Extracellular purines, purinergic receptors and tumor growth. *Oncogene* 2017;**36**:293–303.

58. Pellegatti P, Raffaghello L, Bianchi G. *et al.* Increased level of extracellular ATP at tumor sites: In vivo imaging with plasma membrane luciferase. *PLoS One* 2008;**3**:1–9.
59. Ferrari D, Munerati M, Melchiorri L. *et al.* Responses to extracellular ATP of lymphoblastoid cell lines from Duchenne muscular dystrophy patients. *Am J Physiol* 1994;**267**:C886–C892.
60. Sheng L, Leshchyns'Ka I, Sytnyk V. Cell adhesion and intracellular calcium signaling in neurons. *Cell Commun Signal* 2013;**11**:1–13.
61. Ko KS, Arora PD, Bhide V. *et al.* Cell-cell adhesion in human fibroblasts requires calcium signaling. *J Cell Sci* 2001;**114**:1155–1167.
62. Tsai FC, Kuo GH, Chang SW. *et al.* Ca2+ signaling in cytoskeletal reorganization, cell migration, and cancer metastasis. *Biomed Res Int* 2015;**2015**:1–13.
63. Monteith GR, Prevarskaya N, Roberts-Thomson SJ. The calcium-cancer signalling nexus. *Nat Rev Cancer* 2017;**17**:367–380.
64. Clapham DE. Calcium Signaling. *Cell* 2007;**131**:1047–1058.
65. Prelich G. Gene overexpression: uses, mechanisms, and interpretation. *Genetics* 2012;**190**:841–854.
66. Vachon PH. Integrin Signaling, cell survival, and Anoikis: distinctions, differences, and differentiation. *J Signal Transduct* 2011;**2011**:1–18.
67. Tian DS, Liu J, Chen L. *et al.* The protective effects of PI3K/Akt pathway on human nucleus pulposus mesenchymal stem cells against hypoxia and nutrition deficiency. *J Orthop Surg Res* 2020;**15**:1–9.
68. Izuishi K, Kato K, Ogura T. *et al.* Remarkable tolerance of tumor cells to nutrient deprivation: possible new biochemical target for cancer therapy. *Cancer Res* 2000;**60**:6201–6207.
69. Zhu J, Thompson CB. Metabolic regulation of cell growth and proliferation. *Nat Rev Mol Cell Biol* 2019;**20**:436–450.
70. He Y, Sun MM, Zhang GG. *et al.* Targeting PI3K/Akt signal transduction for cancer therapy. *Signal Transduct Target Ther* 2021;**6**:425.
71. Dogra C, Changotra H, Wergedal JE. *et al.* Regulation of phosphatidylinositol 3-kinase (PI3K)/Akt and nuclear factor-kappa B signaling pathways in dystrophin-deficient skeletal muscle in response to mechanical stretch. *J Cell Physiol* 2006;**208**:575–585.
72. Guo D, Meng Y, Jiang X. *et al.* Hexokinases in cancer and other pathologies. *Cell Insight* 2023;**2**:100077. https://doi.org/10.1016/j.cellin.2023.100077.
73. Jin J, Byun JK, Choi YK. *et al.* Targeting glutamine metabolism as a therapeutic strategy for cancer. *Exp Mol Med* 2023;**55**:706–715.
74. Jin W. The role of tyrosine kinases as a critical prognostic parameter and its targeted therapies in Ewing sarcoma. *Front Cell Dev Biol* 2020;**8**:613.
75. Li RZ, Wang XR, Wang J. *et al.* The key role of sphingolipid metabolism in cancer: new therapeutic targets, diagnostic and prognostic values, and anti-tumor immunotherapy resistance. *Front Oncol* 2022;**12**:941643.
76. Nerlich A, von Orlow M, Rontein D. *et al.* Deficiency in phosphatidylserine decarboxylase activity in the psd1 psd2 psd3 triple mutant of Arabidopsis affects phosphatidylethanolamine accumulation in mitochondria. *Plant Physiol* 2007;**144**:904–914.
77. Liotta LA, Steeg PS, Stetler-Stevenson WG. Cancer metastasis and angiogenesis: an imbalance of positive and negative regulation. *Cell* 1991;**64**:327–336.
78. Ricci S, D'Esposito V, Oriente F. *et al.* Substrate-zymography: a still worthwhile method for gelatinases analysis in biological samples. *Clin Chem Lab Med* 2016;**54**:1281–1290.
79. Toth M, Sohail A, Fridman R. Assessment of gelatinases (MMP-2 and MMP-9) by gelatin zymography. *Methods Mol Biol* 2012;**878**:121–135.
80. Zanotti S, Saredi S, Ruggieri A. *et al.* Altered extracellular matrix transcript expression and protein modulation in primary Duchenne muscular dystrophy myotubes. *Matrix Biol* 2007;**26**:615–624.
81. von Moers A, Zwirner A, Reinhold A. *et al.* Increased mRNA expression of tissue inhibitors of metalloproteinase-1 and -2 in Duchenne muscular dystrophy. *Acta Neuropathol* 2005;**109**:285–293.
82. Anderton J, Moroz V, Marec-Bérard P. *et al.* International randomised controlled trial for the treatment of newly diagnosed EWING sarcoma family of tumours – EURO EWING 2012 protocol. *Trials* 2020;**21**:1–9.
83. Huard J, Labrecque C, Dansereau G. *et al.* Dystrophin expression in myotubes formed by the fusion of normal and dystrophic myoblasts. *Muscle Nerve* 1991;**14**:178–182.
84. Kobayashi T, Ohno S, Park-Matsumoto YC. *et al.* Developmental studies of dystrophin and other cytoskeletal proteins in cultured muscle cells. *Microsc Res Tech* 1995;**30**:437–457.
85. Miranda AF, Bonilla E, Martucci G. *et al.* Immunocytochemical study of dystrophin in muscle cultures from patient with Duchenne muscular dystrophy and unaffected control patients. *Am J Pathol* 1988;**132**:410–416.
86. Park-Matsumoto YC, Kameda N, Kobayashi T. *et al.* Developmental study of the expression of dystrophin in cultured human muscle aneurally and innervated with fetal rat spinal cord. *Brain Res* 1991;**565**:280–289.
87. Trimarchi F, Favaloro A, Fulle S. *et al.* Culture of human skeletal muscle myoblasts: timing appearance and localization of dystrophin-glycoprotein complex and vinculin-talin-integrin complex. *Cells Tissues Organs* 2006;**183**:87–98.
88. Chal J, Oginuma M, Al Tanoury Z. *et al.* Differentiation of pluripotent stem cells to muscle fiber to model Duchenne muscular dystrophy. *Nat Biotechnol* 2015;**33**:962–969.
89. Choi IY, Lim HT, Estrellas K. *et al.* Concordant but varied phenotypes among Duchenne muscular dystrophy patient-specific myoblasts derived using a human iPSC-based model. *Cell Rep* 2016;**15**:2301–2312.
90. Merrick D, Stadler LKJ, Larner D. *et al.* Muscular dystrophy begins early in embryonic development deriving from stem cell loss and disrupted skeletal muscle formation. *Dis Model Mech* 2009;**2**:374–388.
91. Róg J, Oksiejuk A, Gosselin MRF. *et al.* Dystrophic mdx mouse myoblasts exhibit elevated ATP/UTP-evoked metabotropic purinergic responses and alterations in calcium signalling. *Biochim Biophys Acta Mol basis Dis* 2019;**1865**:1138–1151.
92. Ferrari MB, Spitzer NC. Calcium signaling in the developing Xenopus myotome. *Dev Biol* 1999;**213**:269–282.
93. Ewels PA, Peltzer A, Fillinger S. *et al.* The nf-core framework for community-curated bioinformatics pipelines. *Nat Biotechnol* 2020;**38**:276–278.
94. Robinson MD, McCarthy DJ, Smyth GK. edgeR: a Bioconductor package for differential expression analysis of digital gene expression data. *Bioinformatics* 2010;**26**:139–140.
95. Kuleshov MV, Jones MR, Rouillard AD. *et al.* Enrichr: a comprehensive gene set enrichment analysis web server 2016 update. *Nucleic Acids Res* 2016;**44**:W90–W97.
96. Robinson JL, Kocabaş P, Wang H. *et al.* An atlas of human metabolism. *Sci Signal* 2020;**13**:eaaz1482.

97. Thacker JS, Yeung DH, Staines WR. *et al.* Total protein or high-abundance protein: which offers the best loading control for western blotting? *Anal Biochem* 2016;**496**:76–78.
98. Feoktistova M, Geserick P, Leverkus M. Crystal violet assay for determining viability of cultured cells. *Cold Spring Harb Protoc* 2016;**2016**:pdb.prot087379.
99. Cidre-aranaz F. Analysis of migration and invasion in Ewing sarcoma. *Methods Mol Biol* 2021;**2226**:167–179.
100. Hu X, Beeton C. Detection of functional matrix metalloproteinases by zymography. *J Vis Exp* 2010;**45**:e2445.
101. Richardson M, Singh G. Observations on the use of the avian chorioallantoic membrane (CAM) model in investigations into angiogenesis. *Curr Drug Targets Cardiovasc Haematol Disord* 2003;**3**:155–185.
102. Deryugina EI, Quigley JP. Chick embryo chorioallantoic membrane model systems to study and visualize human tumor cell metastasis. *Histochem Cell Biol* 2008;**130**:1119–1130.
103. Ossowski L. In vivo invasion of modified chorioallantoic membrane by tumor cells: the role of cell surface-bound urokinase. *J Cell Biol* 1988;**107**:2437–2445.
104. Tufan AC, Satiroglu-Tufan NL. The chick embryo chorioallantoic membrane as a model system for the study of tumor angiogenesis, invasion and development of anti-angiogenic agents. *Curr Cancer Drug Targets* 2005;**5**:249–266.
105. Zhai Y, Kuick R, Nan B. *et al.* Gene expression analysis of preinvasive and invasive cervical squamous cell carcinomas identifies HOXC10 as a key mediator of invasion. *Cancer Res* 2007;**67**:10163–10172.
106. Marshall KM, Kanczler JM, Oreffo RO. Evolving applications of the egg: chorioallantoic membrane assay and ex vivo organotypic culture of materials for bone tissue engineering. *J Tissue Eng* 2020;**11**:204173142094273.
107. Zatti S, Martewicz S, Serena E. *et al.* Complete restoration of multiple dystrophin isoforms in genetically corrected Duchenne muscular dystrophy patient–derived cardiomyocytes. *Mol Ther Methods Clin Dev* 2014;**1**:1.